Droop Based Control Strategy for an Isolated DC Nanogrid with Boost Type Interfaces

Jingdi Wang

A Thesis

In the Department of

Electrical and Computer Engineering

Presented in Partial Fulfillment of the Requirements

For the Degree of

Master of Applied Science (Electrical and Computer Engineering)

at Concordia University

Montreal, Quebec, Canada

July 2022

CONCORDIA UNIVERSITY

SCHOOL OF GRADUATE STUDIES

This is to certify that the thesis prepared

By: Jingdi Wang

Entitled: Droop Based Control Strategy for an Isolated DC Nanogrid with Boost Type Interfaces

and submitted in partial fulfillment of the requirements for the degree of

Master of Applied Science (Electrical and Computer Engineering)

complies with the regulations of the University and meets the accepted standards with respect to originality and quality.

Signed by the final examining committee:

_____ Chair

Dr. Chunyan Lai

_____ External Examiner

Dr. Mohamed Ouf

_____ Supervisor

Dr. Luiz A. C. Lopes

_____ Supervisor

Dr. Ursula Eicker

Approved by: _____

Dr. M. Zahangir Kabir, Graduate Program Director

Department of Electrical and Computer Engineering

August 3, 2022 _____

Dr. Mourad Debbabi, Dean

Gina Cody School of Engineering and Computer Science

Abstract

Droop Based Control Strategy for an Isolated DC Nanogrid with Boost Type Interfaces

Jingdi Wang

A Nanogrid can integrate Renewable Energy Sources (RESs) easily and power loads locally. DC distribution is more efficient than AC. An isolated DC Nanogrid increases the resilience of a single building, as it can operate in the off-grid mode. Energy storage (ES) units can balance the fluctuating power from RESs and variable load demand.

The considered isolated DC Nanogrid consists of one Photovoltaic (PV) unit, two Energy Storage (ES) units, and multiple loads. Hierarchical control is often used. Decentralized current-mode droop control on the primary level achieves power-sharing. State of Charge (SoC) control avoids overcharging and deep discharging for ES units, working on the slope of droop control on the secondary level. Also, voltage regulation on the secondary level maintains the bus voltage at its nominal value by modifying the "no-load" voltages of droop control for the PV unit and ES units respectively.

Boost-type Class C converters are used as interfaces for ES units. They allow the ES units to have a lower voltage than the bus voltage. The stability issue related to the Right Half Plane (RHP) zero of the Class C converter is analyzed. Based on a worst-case scenario, the controllers are designed to guarantee the system can be stable under considered circumstances. A new design approach for the output capacitor of the converter is introduced to stabilize the system with a random droop factor.

The control strategy is verified in simulations of analog and digital control in different scenarios.

Acknowledgements

I would like to express my deepest appreciation to Prof. Luiz. A.C. Lopes. I deeply appreciate how he has continuously encouraged and guided me and how he has been always so friendly and supportive of my efforts and struggles. His patience in listening to all my rambling ideas and willingness to give suggestions have been very important throughout this process. I continue to learn from him every day, and he never ceases to surprise me with his immense knowledge. Working under his supervision has been very enjoyable.

I am also extremely grateful to Prof. Ursula Eicker. She is brilliant, highly knowledgeable, and enthusiastic about many research fields. Her inspirational leadership, invaluable experience, and innovative ideas always amaze me. I am truly fortunate to have such a supervisor.

I am also thankful to the members of my committee for their time and guidance through the review of the thesis.

I would also like to extend my sincere thanks to my peers on the team of Concordia's Canada Excellence Research Chair (CERC). Their encouragements and experiences have always helped me.

Finally, I would like to express my deepest gratitude to my parents, who have always been supporting me, and to my family for their love and support.

Dedication

This thesis is dedicated to

my father Hongyu Wang and my mother Yunping Xia,

and my family for their love and support.

Table of Contents

List of Figures

List of Tables

Abbreviations

RES: Renewable Energy Source

PV: Photovoltaic

ESS: Energy Storage System

AC: Alternating Current

DC: Direct Current

ES: Energy Storage

SoC: State of Charge

PWM: Pulse Width Modulation

TF: Transfer Function

OP: Operating Point

QOP: Quiescent Operating Point

SC: Supercapacitor

MPPT: Maximum Power Point Tracking

MPP: Maximum Power Point

DOD: Depth of Discharge

BESS: Battery Energy Storage System

HESS: Hybrid Energy Storage System

Chapter 1 Introduction

Climate change and energy shortage-related issues have become more severe in recent years. Thus, reducing the dependence on fossil fuels to decrease carbon emissions has become a focus for researchers and the public. That requires the usage of clean alternatives to fossil fuels, Renewable Energy Sources (RESs) as much as possible, such as solar energy and wind energy. In addition, traditional large-scale centralized power generation needs long-distance transmission lines to supply power to industrial, commercial, and residential buildings. This can lead to line losses and grid vulnerability. If any extreme weather or accident happens along a transmission line, a power outage is likely to occur causing economic losses. A report estimated that power outages cost the U.S. economy $18 billion to $33 billion annually from 2003 to 2012, and another one suggested $25 billion to $70 billion [1].

A smart grid with distributed power generation can be a solution. It can also integrate RESs easily and might not even need the long-distance transmission of electricity. 22 projects were undergoing in the Smart Grid Program of Natural Resources Canada in 2021 nationwide [2].

A Nanogrid is a small-scale smart grid, and it usually refers to a single house or small building [3]. It can easily integrate RESs, such as a solar Photovoltaic (PV) system (roof-installed PV panels) and a small wind turbine producing power locally.

Moreover, an isolated Nanogrid allows a building to work normally even without access to the utility grid in case of power outages increasing its resilience. In that case, an Energy Storage System (ESS) is used to balance the fluctuating power from RESs and variable power demand. For instance, the output power of a PV system constantly changes due to solar radiation. Also, power demand varies based on needs. An ESS usually uses batteries and/or Supercapacitors (SCs) to supply power if there is a power shortage and to absorb surplus power. And a control system is necessary for a Nanogrid to control power flow among multiple energy sources.

Several Nanogrids can form a Microgrid [4]. A Microgrid is a larger-scale grid than a Nanogrid as the name refers and uses similar but more complex techniques. Compared to a Microgrid regarding a community, it is easier to build a Nanogrid for a single house from a socio-economic and technical point of view. The retrofits of homes are boosted all over the world and can be conducted by homeowners with the help of professionals. Canada Greener Homes Initiative offers homeowners

grants to build more energy-efficient homes, including building a PV system and installing batteries connected to the PV system for resilience [5]. Solar PV is becoming the lowest-cost option for power generation in most of the world, according to International Energy Agency [6] and there was a 64% reduction in the residential PV system cost benchmark from 2010 to 2020 with module prices dropping 85% [7]. PV system, therefore, has become a popular choice and makes Nanogrids more feasible.

An isolated Nanogrid can operate normally in the off-grid mode in case of a power failure without access to the utility grid or a Microgrid. Some people have already turned to off-grid homes where extreme weather frequently causes power outages [8]. The off-grid mode should be a more important feature of Nanogrids in the future.

An ESS can balance the power supply and demand in an isolated Nanogrid. A Battery Energy Storage System (BESS) or a Hybrid Energy Storage System (HESS) is commonly employed. The former only uses batteries, and the latter can use batteries and SCs together. Lead-acid batteries have the lowest price but low Depth of Discharge (DOD), short cycle life and low energy density and high maintenance cost. Lithium-ion batteries have a higher price but have a better performance in all other beforementioned characteristics. Lithium Iron Phosphate (LiFePO4) batteries have the lowest toxicity, and they are harder to ignite when mishandled [9]. Thus, they are suitable for Nanogrids. In addition, SCs can respond fast to pulse demand with higher power density, and higher charge/discharge rate than batteries [10]. A HESS can be employed in Nanogrids where batteries with high energy density can supply power in the long term, and SCs can perform in a short period to reduce irregular charge/discharge of batteries slowing down the degradation of batteries.

Nanogrid can be realized in AC (Alternating Current), DC (Direct Current), or Hybrid AC-DC [11]. AC Nanogrids can access the utility grid and power household appliances directly since the appliances in the market are usually powered by the AC utility grid nowadays. However, a DC Nanogrid is regarded as superior to an AC Nanogrid in some aspects. A DC Nanogrid does not need to deal with frequency and reactive power issues as a traditional AC grid does. It needs a less complex control strategy. Most modern household appliances can be powered by DC, and the AC power from the utility grid actually has to be converted into DC before being supplied to these appliances. And during the conversion between AC and DC, power efficiency is decreased [12].

An ESS and a PV system both output DC power. Even a wind turbine whose output power is in AC still needs converting from AC to DC and then possibly back to AC before transmission. If a DC Nanogrid is employed, conversion between AC and DC will be avoided, and thus overall efficiency should increase. A hybrid AC-DC Nanogrid can benefit from both AC and DC Nanogrids but has a more complicated control strategy [13].

1.1 Problem Statement and Proposed Solution

The considered isolated DC Nanogrid is composed of one PV unit, two Energy Storage (ES) units, and five resistive loads in the thesis. In a DC Nanogrid, each energy unit needs to know how much power it needs to supply or absorb based on the load demand at a certain point. Thus, the first control object is to achieve load-sharing (power-sharing) among multiple energy sources in the Nanogrid. In case of communication failure, decentralized control or distributed control can be used here instead of centralized control [14]. Decentralized droop control is popular, and it can generate a reference of the output power for each unit. It can be realized on the primary control level. However, droop control can introduce deviation of the bus voltage which will be regulated on the secondary control level. A two-layer hierarchical control strategy is used in the thesis.

Hierarchical control is commonly used in Nanogrids. Primary control usually deals with autonomous power-sharing without communication in case it fails. Secondary control achieves accurate power sharing and/or bus voltage regulation in a DC grid. Tertiary control concerns optimization and scheduling on a system level [15].

There are two basic types of droop control: current mode and voltage mode [16]. Many papers have discussed voltage-mode droop control with a cascaded loop and two controllers [17]. However, current-mode droop control only needs a single control loop and only one controller for a simpler control design and less computation time. Thus, current-mode droop control is employed here.

Although current-mode droop control might destabilize the system, a new design approach for the output capacitor in the chosen interface is introduced and can properly solve the problem. In addition, controllers are designed to stabilize the system based on the worst-case scenario. The stability of the system under considered conditions can be guaranteed.

The power quality of a DC Nanogrid mainly refers to the bus voltage regulation. Voltage regulation on the secondary control level can maintain the bus voltage at its nominal value at steady state through communication [18]. Voltage regulation sends the same offset signal from secondary control to all energy sources working on their droop control and thus modifying their output power. For instance, if the bus voltage is smaller than the nominal value, the bus voltage can increase to its nominal value with an increase in power in the Nanogrid.

In an isolated DC Nanogrid, there might be overvoltage and undervoltage conditions beyond the capability of voltage regulation. Droop control of the PV unit can help avoid the overvoltage scenario since it defines a maximum accessible bus voltage. For undervoltage cases, Undervoltage Load Shedding can shed non-essential loads to guarantee the normal operation of essential loads, which is not discussed here [19]. Also, Fuel Cells can be used as long-term backup storage, which is also not discussed [20].

The degrading of energy storage depends on its operations, including the number of cycles, State of Charge (SoC) etc., for both batteries [21] and SCs [22]. To prevent energy storage from damaging and aging, SoC control is employed on the secondary control level herein. SoC control can balance the SoC of multiple ES units where the ES units with larger SoC supply more power. It can be realized by working on the slope of the droop line (droop factor) [23]. It is also important that SoC control can keep the SoC of ES units within a safe range. It stops them from discharging at a lower limit and from charging at an upper limit. To achieve the two goals, SoC control is realized by a current gain modifying the droop factor and then the output power of ES units in this thesis [24]. For instance, the output power can be zero at the lower limit while discharging. Also, an alternative method can modify the no-load value of droop control by an offset signal [25] where it refers to the no-load voltage in current-mode droop control. In this project, only SCs are used as ES units to test the control strategy for simplicity.

To summarize, the employed control strategy is two-layer. Primary control uses current-mode droop control to achieve power-sharing. Secondary control regulates the DC bus voltage and controls SoC of ES units with communication.

An isolated DC Nanogrid has more relaxed constraints than the traditional utility grid [26]. Also, due to a lack of standardization, the nominal value of the home distribution voltage (bus voltage) is set from 12VDC to 800VDC in the literature [27]. The most discussed values are 12V, 24V, and

48V. And they are also the most commonly accepted in the market [28, 29]. Considering the level of power consumption in a house and the system complexity, 48V is chosen in this thesis [30]. Many household appliances can use 48V as an input voltage after modification, such as air conditioners, microwave ovens, refrigerators, etc., [31]. The single-bus structure is more suitable for low-voltage DC Nanogrids than the multi-bus structure etc. [32]. Thus, the single-bus structure is employed herein.

Regarding interfaces for energy sources, many publications have preferred buck converters for simplicity. However, PV units, ES units (batteries), and fuel cells have lower voltages than the bus voltage naturally. The parallel arrangement of PV units has less impact on power generation than the series arrangement, and the voltage of a PV unit usually varies from 12 to 36V [33]. Thus, Boost or Buck-Boost converters are considered in a DC Nanogrid.

On the other hand, Boost or Buck-Boost converters might destabilize the system due to Right Half Plane (RHP) zeros if controllers are not properly designed. Some newly designed converters can eliminate the RHP zero but need additional elements [34]. An RHP zero mainly limits the bandwidth. However, secondary control already uses low-bandwidth communication and does not require a fast response. Thus, conventional Class C bidirectional Boost-type converters are used for ES units in this thesis. The worst-case scenario of the Nanogrid, which has the smallest stability margin, is chosen to be the Quiescent Operating Point (QOP) for the control design. Therefore, the system can be stable under considered circumstances.

1.2 Thesis Contribution

1. A control strategy for an isolated DC Nanogrid is designed based on droop control. And it is validated in simulations of analog and digital control.

2. A new design for the output capacitor of a Class C Boost-type converter is introduced, considering current-mode droop control for stability.

3. A new simplified PV model for simulation is introduced.

4. An analysis of the RHP zero in a Class C converter is presented and validated.

5. A current gain is introduced to achieve accurate power-sharing in current-mode droop control for the Boost converter of ES units.

6. Two models of an isolated DC Nanogrid are compared.

1.3 Thesis Outline

Chapter 2 presents the design and analysis of the considered isolated DC Nanogrid, including the configuration of the Nanogrid, current-mode droop control for ES units and a PV unit, and a simplified PV model for simulation. A design approach for droop parameters is presented.

Chapter 3 introduces the design of the primary controller for an ES unit with a Boost-type Class C converter. Voltage-mode and current-mode droop control are compared. The stability issue due to current-mode droop control is analyzed, and a new design method for the output capacitor of the Class C converter is introduced as a solution. The controller is designed based on the worst-case scenario due to an RHP zero. And it is validated in MATLAB and SIMULINK in step responses. A dynamic current ratio is mentioned to achieve accurate power-sharing in droop control.

Chapter 4 discusses secondary control of the isolated DC Nanogrid including voltage regulation and SoC control. The design of the secondary controller is presented. Two models of the DC Nanogrid are compared.

Chapter 5 presents the simulation results of analog control in different scenarios to validate the control strategy as well as the simulation results of digital control.

Chapter 6 highlights the conclusions of the thesis and suggests future work.

Chapter 2 Design and Analysis of Isolated DC Nanogrid

This chapter discusses the configuration of the isolated DC Nanogrid and briefly introduces its hierarchical control strategy: primary control (droop control); secondary control (SoC control and voltage regulation). Power-sharing in primary droop control is discussed based on load variations and variations of the output power of the PV unit. A design approach for droop parameters is discussed here. A simplified PV model for simulation is also introduced.

2.1 Configuration of Isolated DC Nanogrid

The proposed isolated DC Nanogrid consists of one Photovoltaic (PV) unit, two identical Energy Storage (ES) units (ES unit 1 and ES unit 2), and five identical resistive, as shown in Fig 2.1. They are all connected to a single DC bus.

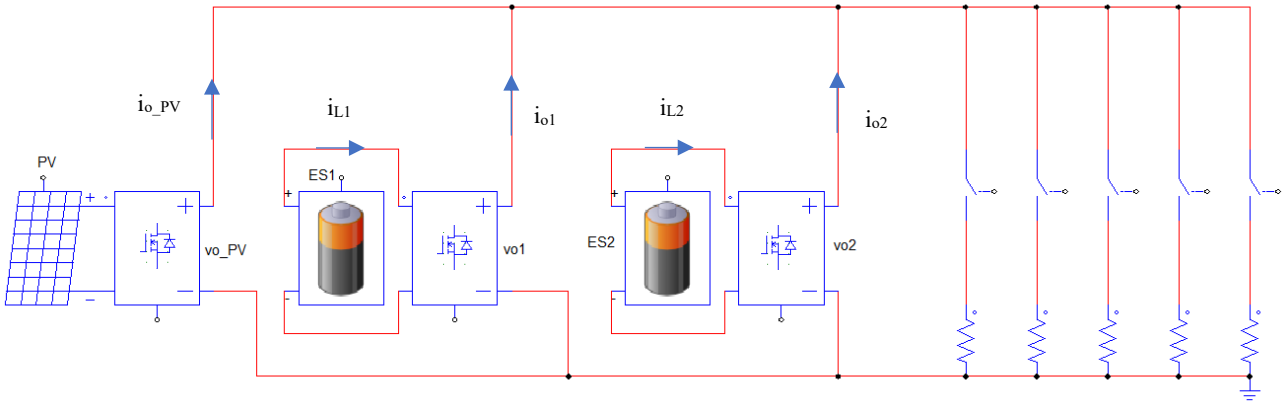

Fig 2.1 Diagram of the considered isolated DC Nanogrid

The PV unit, its interface to the DC bus, and its controller are combined and simplified into one model for simulation discussed in Section 2.3. The interfaces of ES units are Class C DC-DC converters. Feeder impedances are neglected. Assume that all output voltages of interfaces are the same as the load voltage.

The power supply from PV and power demand of the loads are variable in the Nanogrid. The maximum power of the PV unit changes based on solar irradiation and other environmental factors. Maximum Power Point Tracking (MPPT) makes PV supply the maximum power [35]. Meanwhile,

load demand can also vary, determined by the number of switched-on loads. ES units are used to balance the fluctuating power supply from the PV unit and the variable power demand of loads and to obtain good power quality, i.e., a stable DC bus voltage.

Two-layer hierarchical control is employed, as shown in Fig 2.2. Primary control achieves autonomous power-sharing among multiple power sources, PV and ES units, without communication. It determines the amount of power for each unit and has the bus voltage within a designed range using droop control. Primary control also includes SoC control of ES units. Secondary control regulates the bus voltage.

In droop control, the local output voltages are measured, v_{o_pv}, v_{o1}, and v_{o2} in Fig 2.1. Output current references I_o^* are then generated. Thus, a reference of the output power of each unit is generated and will be followed, achieving power-sharing. Droop control uses but also introduces deviation of the bus voltage. For ES units, droop control includes droop mode and current limit, as shown in Fig 2.3. For the PV unit, droop control includes MPPT mode, droop mode, and current limit. The current limits are designed based on the rating currents of the device and the maximum power of each unit. k_{ioL} is a dynamic current ratio for each ES unit between i_L and i_o. Thus, the inductor current i_L can be controlled provided the reference of output current I_o^* for an ES unit. And it guarantees accuracy power-sharing where the actual i_o follows I_o^*.

SoC control of ES units on the primary control level avoids overcharging and deep discharging for safety concerns. It keeps SoC within its boundaries. It can also balance the SoC of multiple ES units. SoC control is realized by a current factor k_{SoC}, working on the generated current reference I_o^* in droop control. If an ES unit approaches its upper or lower limit of SoC, the value of the new current reference will be reduced as well as the output power.

Bus voltage regulation control (secondary control) needs one-way communication from the secondary controller to each unit. It sends a control signal δv to all units changing the "no-load" voltages in the original droop control for all energy sources. δv is calculated based on the local bus voltage (load voltage) v_o in the secondary controller. Given proper SoC of ES units, the DC bus voltage can be regulated at the nominal value V_{nl}.

The details of the control strategy are discussed in the following sections.

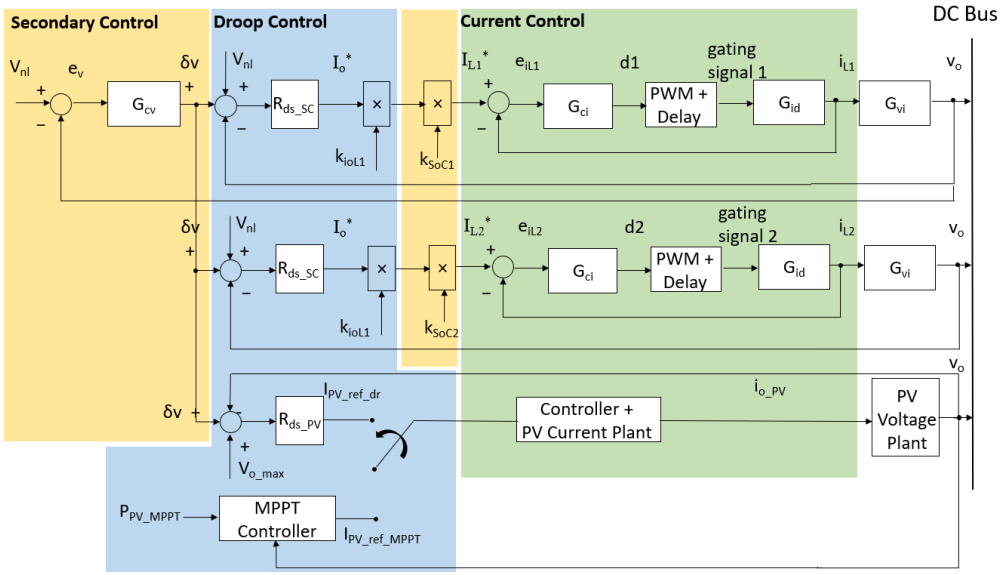

Fig 2.2 Control scheme

R_{ds}: droop factor, G_{cv}: voltage regulator/secondary PI controller; G_{ci}: current PI controller; PWM: Pulse Width Modulation; Delay: delay due to sensors and control computation; G_{id}: plant transfer function from duty cycle to the inductor current; G_{vi}: plant transfer function from the inductor current to the bus voltage.

2.2 Current-mode Droop Control of PV and ES units

Fig 2.3 shows droop curves for an ES unit and a PV unit. The output voltages of the converters are measured, v_{o_PV}, v_{o1}, *and* v_{o2} in current-mode droop control in Fig 2.1. They all equal to the bus volage v_o since the cable impedances are neglected here.

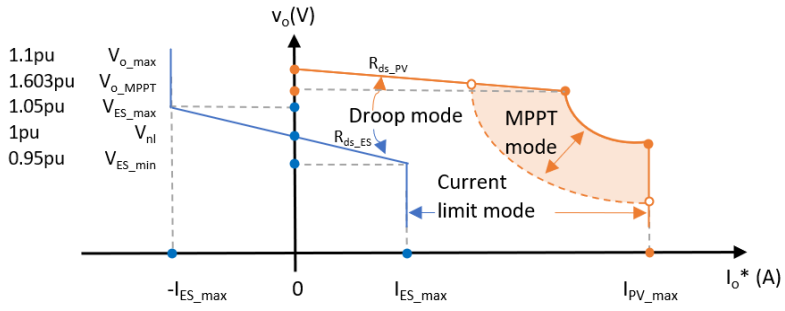

Fig 2.3 Droop curves for an ES unit (blue) and PV unit (orange)

v_o is the actual bus voltage. I_o^* is the reference of the output current of an interface. I_o^* is generated solely based on the measured bus voltage v_o, and thus droop control determines the reference of output power for each unit $P_o^* = v_o I_o^*$. Powe-sharing can be achieved. The details will be discussed in the following section.

A current controller is designed to make i_o follow I_o^* for ES units discussed in Chapter 3. Communication is unnecessary here. This distributed control method guarantees the normal operation of the DC Nanogrid if communication failure happens.

V_{o_max} and V_{nl} are the intersections on the vertical axis for the PV and ES units respectively, and thus "no-load" voltages. V_{nl} is the nominal value of the bus voltage. V_{o_max} is the maximum value that the bus voltage can reach in droop control. V_{o_MPPT} is the minimum voltage in the droop region for the PV unit. V_{ES_max} and V_{ES_min} are the maximum and minimum voltages in the droop region for an ES unit.

R_{ds_PV} and R_{ds_ES} are droop factors and slopes of the droop curves. The current limits are $\pm I_{ES\_max}$ for an ES unit and I_{PV_max} for the PV unit.

For an ES unit, droop control has two modes: droop mode; current limit with $\pm I_{ES\_max}$. If the current is positive, the ES unit is supplying power to the Nanogrid; if negative, absorbing power from the Nanogrid. Due to the values of parameters, the output power increases with a larger positive I_o^* and a smaller v_o for an ES unit in the droop region. The ES unit works as a current source in current limit mode. When $I_{o\_ES}^*$ is expressed as a function of v_o, it is as below.

$$\text{ES unit: } I_{o\_ES}^* = \begin{cases} \text{positve current limit: } I_{ES\_max}, & \text{if } v_o \le V_{ES\_min} \\ \text{droop: } \frac{-v_o + V_{nl}}{R_{ds\_ES}}, & \text{if } V_{ES\_min} < v_o < V_{ES\_max} \\ \text{negetive current limit: } -I_{ES\_max}, & \text{if } v_o \ge V_{ES\_max} \end{cases}. \quad (2.1)$$

Regarding the PV unit, it is the main energy source. Due to the photovoltaic effect, a photovoltage is generated on a solar cell which is its output voltage. When the external circuit is short-circuited, the output current of the solar cell is short-circuit current I_{SC}, and when it is open-circuited, the output voltage is open-circuit voltage V_{OC} [36]. Their relationship is shown below. According to the solar radiation at a certain time, there is a maximum value of the output power of the solar cell at Maximum Power Point (MPP). Maximum Power Point Tracking (MPPT) control can make the cell output the maximum power which will not be discussed in this thesis. When several solar cells

are arranged in series and parallel, they form a solar panel. And the PV unit can be obtained by having several solar panels in series for efficiency.

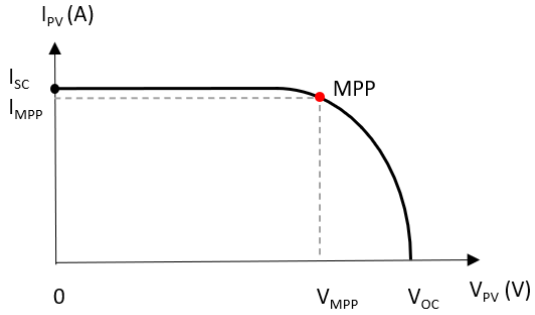

Fig 2.4 I-V characteristic curve of a solar cell

Assume that all solar cells are working under the same condition and have the same I-V curve. Then the output current should be multiple times of I_{MPP} working on MPP as well as the voltage of the PV unit of V_{MPP}. For simplicity, assume Fig 2.4 is the I-V curve for the PV unit. The output voltage of the PV unit becomes V_{PV}, and it is also the input voltage of its converter. The output voltage of the converter is v_o in droop control in Fig 2.3.

For a PV unit, it has three control modes in droop control: droop mode, MPPT mode, and current limit. Since the PV unit is preferred to work in MPPT mode to benefit most from the RES, it is designed to work in MPPT mode most of the time. Thus, the point MPP of the PV unit in Fig 2.4 refers to a large range of v_o in Fig 2.3, the MPPT region. The output power of the PV unit is the constant maximum power p_{MPPT}, but the bus voltage and the output current can vary. Once P_{MPPT} changes, a new MPPT segment forms, as shown in Fig 2.3.

The PV unit can only supply power, and thus its reference of output current is positive. The relationship between $I_{o\_PV}{}^*$ and v_o in droop mode: $I_{o\_PV}{}^* = \frac{-v_o + V_{omax}}{R_{dr\_PV}}$, if $V_{ES\_min} < v_o < V_{ES\_max}$. And the other modes will be discussed in Section 2.3. The power increases with a decrease in the bus voltage in droop mode.

It is noted that droop control uses deviation of the bus voltage, and it also introduces the deviation. Secondary control can help with this issue. Bus voltage regulation keeps the DC bus voltage at V_{nl} discussed in Chapter 4. If it reaches its limit, where it can no longer regulate the voltage, there are two conditions. In an overvoltage scenario with small load demand, $v_o > V_{nl}$ and the PV unit supplies power to the loads and ES units. v_o is smaller than V_{o_max} at any condition. The output

power of the PV unit is 0 with all loads shut down at V_{o_max}. In undervoltage scenarios, another control method, such as Undervoltage Load Shedding, can be used. Or backup storage such as fuel cells should be used. These two are not mentioned in this thesis.

2.2.1 Power-sharing in DC Nanogrid with primary control

a. Load variation

Fig. 2.5 shows the change of the Operating Points (OPs) of the proposed DC Nanogrid with a change in load demand. There are two identical ES units in the Nanogrid and assume that they output the same amount of current with the same bus voltage v_o. Combine them into one large ES unit with twice the current limits $\pm 2I_{ES\_max}$ and a half droop factor $\frac{k_{ds\_ES}}{2}$ in blue. DERs with two ES units in blue and one PV unit in orange are then combined into one curve in green. Since there is unlikely to not have any load in the Nanogrid, the left half plane of the green curve is not drawn, and the no-load condition will not be discussed.

The load is resistive, $i_{load} = \frac{v_o}{R_{load}}$, and thus they can be represented by straight lines in yellow. Assume that the controllers are well designed, $i_o = I_o^*$ for each unit at steady state for the following analysis.

When $R_{load} = R_{o1}$, the OP of the Nanogrid is at OP1 on the Right Half Plane (RHP). It is the intersection of the green curve and the load R_{o1} line since they share the same output/bus voltage, and the total output current of sources equals the load current. The PV unit is working in the MPPT mode at point $PV_{\_1}$. And two ES units are charging at $ES_{\_1}$ with current $\frac{i_{ES\_1}}{2} < 0$ for each.

And then, the load changes to R_{o2}, and the OP becomes OP2, sliding along the green curve. PV unit still works in the MPPT mode at $PV_{\_1}$, supplying the same amount of power but with different bus voltage and output current. However, since the load demand increases, the ES units need to supply power at point $ES_{\_2}$, discharging with current $\frac{i_{ES\_2}}{2} > 0$ for each.

Power demand is thus shared among multiple units. The dispatching ratio is determined by droop parameters, such as the slope and the "no-load" voltage for each unit, which will be discussed in 2.2.2.

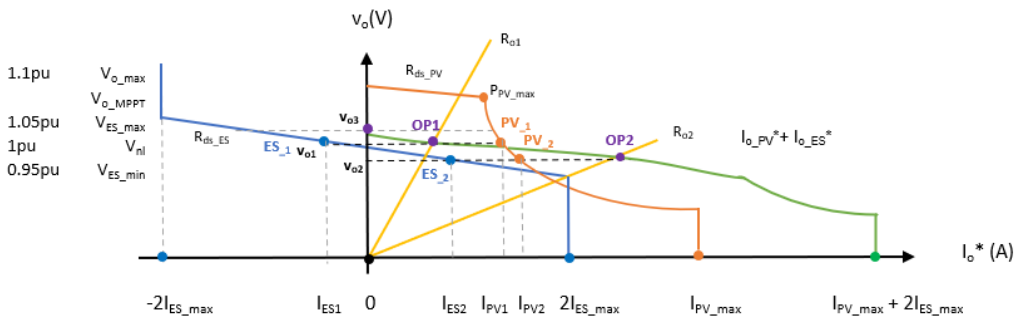

Fig 2.5 Change of operating points with a varied load demand

b. p_{MPPT} variation

Fig 2.6 shows the scenario where the maximum power of PV unit, p_{MPPT}, changes. p_{MPPT} fluctuates due to environmental factors. If p_{MPPT} reduces, a new MPPT segment is formed in the dashed orange curve. The green curve changes accordingly to the dashed green curve. The operating point changes to OP3 from OP2 sliding along the load R_{o2} line. The load has not changed. PV unit still works in the MPPT mode but supplies less power at PV_3. ES units have to supply more power at ES_3 with a larger output current.

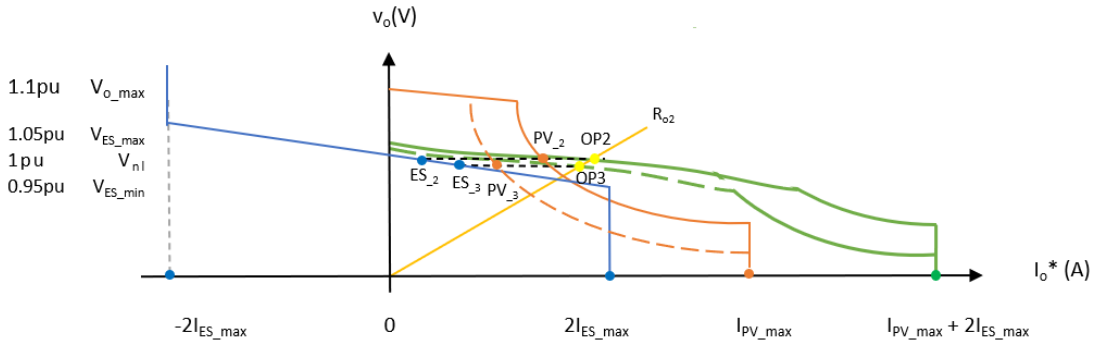

Fig 2.6 Change of operating points with a varied P_{MPPT}

To summarize, droop control can achieve power/load-sharing among multiple energy sources in different scenarios with variable load demand and fluctuating RES power. The output power of each unit is determined by parameters of droop control.

2.2.2 Design approach for droop control parameters

To guarantee the power from the RES is fully used, the PV unit is made to work in MPPT mode for most of the time. This can reduce the discharging currents of ES units and thus the rate of charge and discharge to prolong their life cycles. Therefore, the PV unit should have a higher priority than

ES units in terms of supplying power. If ES units are discharging, MPPT must be made to work in MPPT mode supplying the maximum power.

Furthermore, the PV unit should also work in the MPPT mode when ES units absorb power and reach the maximum current of $-I_{ES\_max}$. Then with an increasing bus voltage, the PV unit may enter the droop region. Since the proposed Nanogrid is isolated without access to the utility grid, to ensure sufficient power in the future, ES units should be maintained at high-level SoC. If the PV unit, working in MPPT mode, charges the ES units with the maximum current, the charging time can be the shortest with certain solar radiation. Otherwise, the PV unit will work in the droop region while the ES units are charged with the maximum current, or the PV unit is working in the MPPT region while the ES units are charged with a smaller current. The charging time in these two scenarios should be longer than the first case.

In summary, during the entire range of droop control of ES units from $-I_{ES\_max}$ to I_{ES_max}, the PV unit should always work in the MPPT mode in the original droop control.

Additionally, load demand is considered in the parameter design. However, in the realistic scenario, current limits are also designed based on the maximum device current, such as converters, cable, batteries, etc. Also, the cost needs considering. Those two are not considered here.

a. Voltage parameters

The nominal bus voltage V_{nl} is set 48V. The overall maximum voltage $V_{o_max} = 48 \times 1.1 = 52.8$V, the maximum bus voltage of ES units in droop region $V_{ES_max} = 48 \times 1.05 = 50.4$V, and the minimum bus voltage of ES units in droop region $V_{ES_min} = 48 \times 0.95 = 45.6$V. The entire range of the bus voltage in droop region is from 45.6V (0.95pu) to 52.8V (1.1pu), 0.95 to 1.1 of V_{nl} at steady state.

The output power in MPPT mode p_{MPPT} varies with the maximum power point (MPP) of the PV unit. That can be presented by the changing MPPT curve with the intersection of the droop line and the MPPT curve sliding along the droop line, as shown in Fig 2.3. When the PV unit obtains its rated maximum output power, where $p_{MPPT} = P_{PV\_max}$, the intersection has the minimum voltage V_{o_MPPT}, and it is determined by P_{PV_max}. P_{PV_max} is the maximum value of p_{MPPT} at all MPPs.

To make sure that the PV unit works in MPPT mode, and it can always charge ES units at $-I_{ES\_max}$ at any MPP, it is necessary that $V_{o\_MPPT} > V_{ES\_max}$. In other words, the PV unit can only enter droop

mode supplying less power after ES units are charged with I_{ES_max} in the current limit mode. Also, $V_{o\_MPPT} < V_{o\_max}$. Thus, $V_{ES\_max} < V_{o\_MPPT} < V_{o\_max}$. Set V_{o_MPPT} = 51V (1.063pu).

b. Other parameters considering load demand

1) I_{ES_max}, maximum powers, and droop factors

There are five identical resistive loads of 24Ω in the Nanogrid, and R_{o_min} = 4.8Ω. The maximum load power $P_{load_max} = \frac{{V_{nl}}^2}{R_{o_min}} = 480$W at V_{nl} considering secondary control. The maximum power of an ES unit P_{ES_max} is set to be 240W at V_{nl}. Thus, two ES units can satisfy the maximum power demand in the absence of the PV unit for some time. The current limit $I_{ES\_max} = \frac{P_{ES\_max}}{V_{nl}} = 5A$. The droop factor of ES units R_{ds_ES} = 0.48V/A.

The PV unit should cover the maximum load demand, where $P_{PV\_max} > P_{load\_max}$, but not necessarily also cover the maximum charging power of two ES units at the same time ($P_{load\_max} + 2P_{ES\_max} =$ 960W). However, P_{PV_max} can be set close to 960W, $P_{PV\_max} \approx P_{load\_max} + 2P_{ES\_max}$. If $P_{PV\_max} >$ 960W, the PV unit might never reach its maximum capacity. Thus, set $P_{PV\_max} <$ 960W. Set P_{PV_max} = 800W. $I_{PV}^{*} = \frac{P_{PV\_max}}{V_{o\_MPPT}} = 15.69A$ at the intersection of droop and MPPT region with the maximum power P_{PV_max}. The droop factor of PV unit R_{ds_PV} = 0.115V/A.

2) I_{PV_max}

As mentioned before, the PV unit should be able to work in the MPPT mode in the entire droop region of the ES units. V_{o_MPPT} satisfies that while the ES units are charging. Now the discharge of the ES units is discussed. If the PV unit can work in the MPPT mode with P_{PV_max} and at the same time the ES units are discharging with I_{ES_max} at V_{ES_min}, the PV unit can work in MPPT mode with any given p_{MPPT} while the ES units are discharging with I_{ES_max}.

Thus, the intersection of MPPT mode and the current limit on the PV curve: $v < V_{ES\_min}$. Thus, $\frac{P_{PV\_max}}{I_{PV\_max}} < V_{ES\_min}$. And $I_{PV\_max} > \frac{P_{PV\_max}}{V_{ES\_min}}$. Therefore, $I_{PV\_max} > 17.54A$. Set $I_{PV\_max} = 18A$.

Table 2.1 Parameters in droop control

Parameter	Symbol	Value	Unit
Droop factor of PV unit	R_{ds_PV}	0.115	V/A
Droop factor of the ES units	R_{ds_ES}	0.48	V/A
Max DC bus voltage	V_{o_max}	52.8 (1.1)	V (pu)
Min droop voltage of the PV unit	V_{o_MPPT}	51(1.063)	V (pu)
Max droop voltage of the ES units	V_{ES_max}	50.4 (1.05)	V (pu)
No-load/rated DC bus voltage	V_{nl}	48 (1.0)	V (pu)
Min droop voltage of the ES units	V_{ES_min}	45.6 (0.95)	V (pu)
Current limit of the PV unit	I_{PV_max}	18	A
Current limit of the ES units	I_{ES_max}	+/-5	A

2.3 Simplified Model of PV Unit for Simulation

The droop control of the PV unit includes three modes: droop, MPPT, and current limit. Thus, the control strategy of the PV unit includes two methods: MPPT control and droop control. Current limit can be easily realized by a limiter clamping the reference of its output current.

MPPT mode is used to track the Maximum Power Point (MPP) and ensures the PV unit outputs the maximum power based on the current solar radiation. On the other hand, droop mode enables the PV unit to output a certain amount of power calculated from the droop curve, smaller than the maximum power. It is possibly activated if there is small load demand. Only one control method is enabled at a time, and it is based on the measured output voltage.

An actual PV unit should work together with a unidirectional DC-DC converter and a well-designed controller to control the interface. For simplicity, the three elements are combined into one PV model, as shown in Fig 2.7. Now that a simplified current source-based model can represent the PV unit, its interface, and its controller for simulation in PSIM.

Each current source represents one mode on the droop curve of the PV unit. And only one current source is enabled at a time. The mode is selected by control signals PV_dr, PV_MPPT, and PV_cl. Mode is selected based on the measured bus voltage v_o.

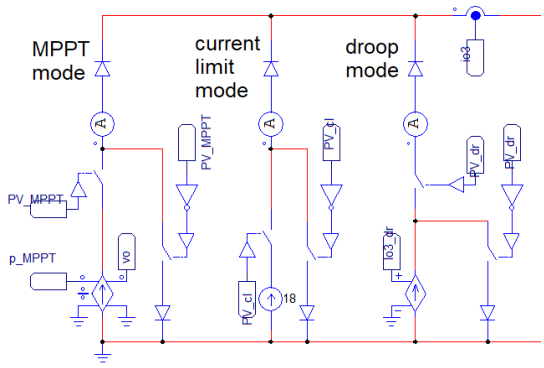

Fig 2.7 Simplified PV model

$v_{o\_MPPT\_uv}$ and $v_{o\_MPPT\_lv}$ are the upper and the lower voltages in MPPT mode on the curve. The former is the intersection of the droop region and MPPT region, and the latter is the intersection of the MPPT region and region of current limit. The two parameters change according to the variable p_{MPPT}. δv is a control signal from the secondary controller, and it is 0 if only the primary control is activated. δv adjusts V_{o_max}, and $V_{o\_max\_new} = V_{o\_max} + \delta v$.

Thus,

$$v_{o\_MPPT\_uv} = \frac{(V_{o\_max}+\delta v)+\sqrt{[(V_{o\_max}+\delta v)^2 - 4\,R_{ds\_PV}\,p_{MPPT}]}}{2}. \tag{2.2}$$

$$v_{o\_MPPT\_lv} = \frac{p_{MPPT}}{I_{PV\_max}}. \tag{2.3}$$

$I_{o\_PV}{}^*$ is the reference of the output current and the actual current in this model. Since the controller of the PV unit is omitted, there is no error between $I_{o\_PV}{}^*$ and i_{o_PV}.

$$i_{o\_PV} = I_{o\_PV}{}^* = \begin{cases} \text{current limit: } I_{PV\_max}, & \text{if } v_o \le V_{o\_MPPT\_lv} \\ \text{MPPT: } \frac{p_{MPPT}}{v_o}, & \text{if } V_{o\_MPPT\_lv} < v_o < V_{o\_MPPT\_uv} \\ \text{droop: } \frac{-v_o + V_{omax\_new}}{R_{dr\_PV}}, & \text{if } v_o \ge V_{o\_MPPT\_uv} \end{cases} \tag{2.4}$$

If $v_o \ge v_{o\_MPPT\_uv}$, the interface operates in the droop mode. If $v_o \le v_{o\_MPPT\_lv}$, the interface operates in current limit. Otherwise, the PV unit is in MPPT mode. It is implemented in PSIM, as shown in

Fig 2.8. It can also simulate the scenarios in which p_{MPPT} varies. And the droop curve with the latest p_{MPPT} can update automatically using this model.

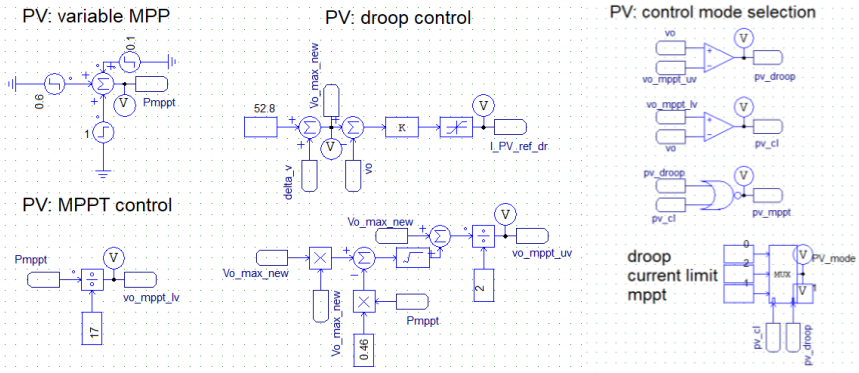

Fig 2.8 Mode selection of PV unit in simulation

Chapter 3 Design of Primary Control for ES units

This chapter discusses the design of primary control for an ES unit. The Class C converter is chosen as the interface. Current-mode droop control is used as the primary control method. It only needs a single loop, and thus only one current controller is designed.

Due to the Boost Class C converter, there is a Right Half Plane (RHP) zero in the plant transfer function. To guarantee the stability of primary control at different operating points, a worst-case scenario is chosen to be the Quiescent Operating Point (QOP) based on which the current controller is designed. Furthermore, since there is no controller for the output voltage of the converter in current-mode droop control, the output capacitor of the converter is redesigned to stabilize the bus voltage with a predefined settling time.

To verify the stability of the closed primary control loop, its step responses are tested with the secondary control signal and with load variation respectively. A current gain is employed in simulations to achieve accurate power-sharing at steady state.

3.1 Bidirectional Class C DC-DC Converter

The Class C DC-DC converter is chosen to be the interface for an ES unit connecting to the DC bus. It is a bidirectional converter (inductor current i_L and output current i_o) and allows the ES unit to charge and discharge. It comprises two switches, one input inductor L, and one output capacitor C_o, as shown in Fig 3.1.

A Class C converter works in the Boost mode while discharging and supplying power to the bus and the load with positive currents i_L and i_o (the same directions as those in Fig 3.1) and in the buck mode while charging and absorbing power from the bus with negative i_L and i_o (the opposite directions to those in Fig 3.1). v_{ES} is the voltage of the ES unit or the input voltage of the converter, R_o is the load, and v_o is the bus/output voltage.

The gating signal of the bottom switch is generated by a PWM (Pulse Width Modulation) module, and its duty cycle is d. The gating signals for the two switches are complementary. Otherwise, the bus is short-circuited.

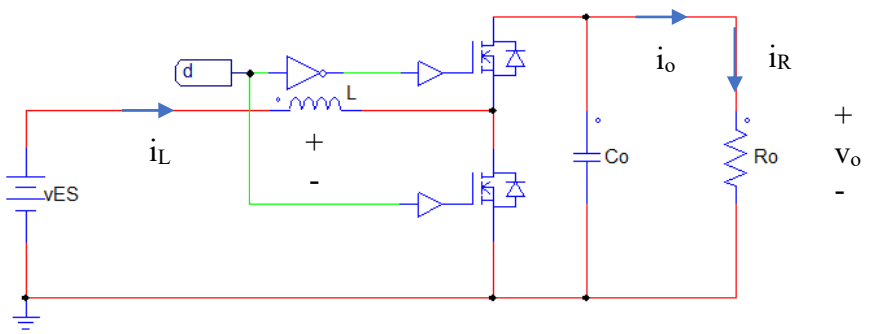

Fig 3.1 Class C converter for an ES unit

3.1.1 Small-signal model and average model in Boost mode

A small-signal model can be obtained by averaging and linearizing around an Operating Point (OP) according to Kirchhoff's Voltage Law (KVL) and Kirchhoff's Current Law (KCL) [37]. For each parameter, its value is the sum of the average value and a small signal, such as $v_o = V_o + \tilde{v}_o$.

The average model is as below.

$$V_o = \frac{V_{ES}}{(1-D)};$$

$$I_o = (1-D)I_L = I_{Ro} = \frac{V_o}{R_o}. \tag{3.1}$$

Transfer functions (TFs) of small signals can be obtained as below.

$$\text{From duty cycle } \tilde{d} \text{ to } \tilde{\imath}_L\text{: } G_{id}(s) = \frac{i_L(s)}{d(s)} = \frac{C_o V_o s + \frac{V_o}{R_o} + I_L(1-D)}{LCs^2 + \frac{L}{R_o}s + (1-D)^2}. \tag{3.2}$$

$$\text{From duty cycle } \tilde{d} \text{ to } \tilde{v}_o\text{: } G_{vd}(s) = \frac{v_o(s)}{d(s)} = \frac{-LI_L s + V_o(1-D)}{LC_o s^2 + \frac{L}{R_o}s + (1-D)^2}. \tag{3.3}$$

Note that there is a Right Half Plane (RHP) zero, $s = \frac{V_o(1-D)}{LI_L} = \frac{R_o(1-D)^2}{L}$ in $G_{vd}(s)$. The smaller the RHP zero is, the larger its impact is.

$$\text{From } \tilde{\imath}_L \text{ to } \tilde{v}_o\text{: } G_{vi}(s) = \frac{v_o(s)}{i_L(s)} = \frac{-\frac{L}{(1-D)}s + R_o(1-D)}{R_o C_o s + 2}. \tag{3.4}$$

Note that the same RHP Zero still exists.

3.1.2 PWM model

The duty cycle for the bottom switch $d(s) = \frac{v_{mod}(s)}{\hat{V}_{tri}}$ for a triangular carrier. $v_{mod}(s)$ is the signal from the primary controller, and the peak value of the triangular carrier $\hat{V}_{tri} = 1$. Thus, $PWM(s) = \frac{d(s)}{v_{mod}(s)} = 1$.

3.1.3 Components selection and calculation

According to State of Charge (SoC) control, the voltage of an ES unit $v_{ES} \in [20, 30]$. The bus voltage $v_o \in [45.6, 52.8]$ due to droop control in primary control. Thus, $D = 1 - \frac{V_{ES}}{V_o} \in [0.342, 0.621]$.

A). Current ratings

The maximum power of an ES unit at the nominal voltage of 48V is ±240W, and the maximum output current is I_{ES_max} = 5A. Thus, I_{L_max} = 13.19A, where D_{max} = 0.621.

B). Calculation of inductance *L*

Set the maximum acceptable ripple of the inductor current ΔI_{L_max} = 2% I_{L_max} = 0.26A.

$v_L = L\ \frac{di_L}{dt} = v_{ES}$ during the on-time of the bottom switch DT_{sw}; $v_L = L\ \frac{di_L}{dt} = v_{ES} - v_o$ during the off-time of the bottom switch $(1 - D)T_{sw}$. Thus, $\Delta I_L = \frac{v_{ES}DT_{sw}}{L} = \frac{(v_o - v_{ES})(1-D)T_{sw}}{L}$. T_{sw} is the switching period.

$$L \geq \left[\frac{v_{ES}DT_{sw}}{\Delta I_{L\_max}}\right]_{max} = \left[\frac{(v_o - v_{ES})(1-D)T_{sw}}{\Delta I_{L\_max}}\right]_{max.} \quad (3.5)$$

Apparently, the maximum value of v_{ES} and D cannot be obtained at the same time. D_{max} is obtained with the lower limit of an ES unit v_{ES_L} and the maximum output voltage v_{o_max}. The same case also happens to the latter expression. It is possible to use the following expression to get the minimum value of L since there is no limiting factor between v_{ES} and v_o.

$$L \geq \left[\frac{v_{ES}(1-\frac{v_{ES}}{v_o})T_{sw}}{\Delta I_L}\right]_{max}. \quad (3.6)$$

Use MATLAB given the constant step of 0.1V for v_{ES} and v_o, and their ranges. $L \geq$ 2.54mH, where $v_{ES} = 26.4V, v_o = 52.8V$, and switching frequency f_{sw} = 20kHz.

C). Calculation of capacitance C_o

$i_C = -i_o$ during the on-time of the bottom switch; $i_C = i_L - i_o$ during the off-time of the bottom switch. And $i_C = C_o \frac{dv_o}{dt}$. Thus, $\Delta V_o = \frac{i_o D T_{sw}}{C_o} = \frac{(i_L - i_o)(1-D)T_{sw}}{C_o}$.

Set the maximum acceptable ripple of v_o is $\Delta V_{o\_max} = 2\%\ V_{o\_max} = 1.06\text{V}$, where $V_{o\_max} = 52.8V$.

$$C_o \geq \left[\frac{i_o D T_{sw}}{\Delta V_{o\_max}}\right]_{max} = \left[\frac{(i_L - i_o)(1-D)T_{sw}}{\Delta V_{o\_max}}\right]_{max}. \quad (3.7)$$

The minimum C_o can be obtained when i_o and D have their maximum values respectively. $I_{o\_max} = 5\text{A}$ and $D_{max} = 0.621$. $C_o \geq 146\mu\text{F}$ if $f_{sw} = 20\text{kHz}$.

The used C_o is much larger, and the analysis will be given in the following section.

3.2 Droop Control for ES Units

3.2.1 Droop control: current mode vs. voltage mode

Droop control is chosen to be the primary control method. Although there are two regions on the curve of droop control, droop mode (a straight line) and current limit (two vertical lines), an ES unit is expected to work in the droop mode to have the value of the bus voltage within its range. Thus, only droop mode is considered here.

Droop control includes two basic types: current mode and voltage mode. In the droop region of current-mode droop control, the output voltage of the converter, namely the DC bus voltage v_o neglecting cable impedances, is measured, and the reference of the output current $I_{o\_ES}{}^*$ is generated accordingly. In voltage-mode droop, it is the other way around. The two methods use the same curve and the same parameters. With well-designed controllers, they are supposed to generate the same amount of power at steady state. The control signal from secondary controller $\delta v = 0$ in primary control.

Current mode: $I_{o\_ES}{}^* = \frac{-v_o + V_{nl} + \delta v}{R_{ds\_ES}}$. (3.8)

Voltage mode: $V_o{}^* = -i_{o\_ES} R_{ds\_ES} + V_{nl} + \delta v$. (3.9)

For current-mode droop control, the primary loop for an ES unit just needs a single inner current controller $G_{ci}(s)$ (a single loop), and for voltage-mode, an inner-current controller $G_{ci}(s)$ and outer-voltage controller (a cascaded dual loop), as shown in 3.2. The control strategy of current-mode droop is simpler and needs a shorter computation time. Current-mode droop control is employed herein.

On the other hand, there is an additional voltage controller to stabilize the output/bus voltage in voltage mode. Current-mode droop control however may encounter voltage instability issues. It can be dealt well with a properly designed output capacitor of an ES unit, C_o. The design approach is discussed in the next section.

Since the output current i_{o_ES} cannot be controlled directly due to the topology of the Class C converter, the inductor current i_L is controlled instead. A dynamic ratio is used, $k_{ioL} = \frac{I_{L^*}}{I_{o\_ES^*}} = \frac{v_o}{v_{ES}}$, where v_o and v_{ES} are measured . Note that only at steady state, $i_o = k_{ioL} i_L$. Also, k_{ioL} represents the voltage gain.

$K_{ioL} = \frac{1}{1-D}$ is a constant based on a chosen Quiescent Operating Point (QOP) for control design. d is the duty cycle, e_v is the error of DC bus voltage, $I_L{}^*$ is the reference of the inductor current, and e_{iL} is the error of the inductor current. V_{nl} is a constant (DC value) and thus omitted. Moreover, all signals in control diagrams and transfer functions are small signals or variations and thus expressed as $\tilde{\delta v}, \tilde{\imath}_L$ and $\tilde{v}_o$. δv is the control signal from secondary control. $\delta v = \Delta V + \tilde{\delta v}$, ΔV is a DC value at QOP and omitted. To keep the small signals of parameters, the control diagrams are as below.

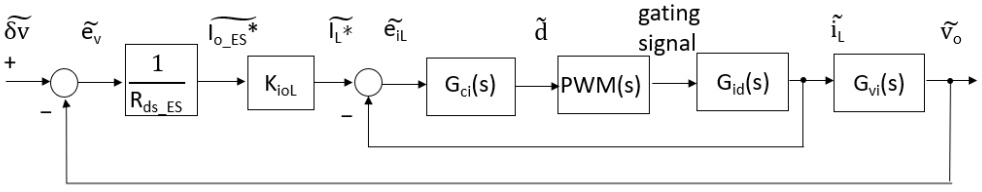

Fig 3.2.a) Control diagram of current-mode droop with secondary control signal $\tilde{\delta v}$

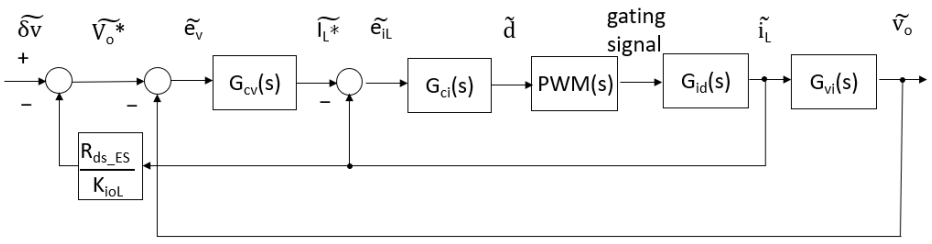

Fig 3.2.b) Control diagram of voltage-mode droop with secondary control signal $\tilde{\delta v}$

3.2.2 Stability issue in current-mode droop control

A). RHP zero

If an ES unit is supplying power, its converter is working in Boost mode. And if it is absorbing power, its converter is in buck mode. And there is a Right Half Plane (RHP) zero in the Boost mode in $G_{vd}(s)$ and $G_{vi}(s)$. The former is the TF from the duty cycle $\tilde{d}$ to output voltage $\tilde{v}_o$, and the latter from the inductor current $\tilde{\imath}_L$ to $\tilde{v}_o$.

$G_{vi}(s)$ appears in the control diagram in Fig 3.2.a). The RHP zero may destabilize primary control, especially because the only controller $G_{ci}(s)$ will not impact the performance of $\tilde{v}_o$. Therefore, to guarantee the system can stabilize at any operating point within a predefined range, $G_{vi}(s)$ should be obtained based on the Boost mode of the converter considering the worst-case scenario. The smaller the RHP zero, the larger its impact is. Therefore, the worst-case scenario is obtained when the RHP zero is the smallest.

RHP Zero: $z_{RHP} = \frac{V_o(1-D)}{LI_L} = \frac{R_o(1-D)^2}{L}$. (3.10)

B). QOP

Current controller $G_{ci}(s)$ uses PI type II controller and is designed based on the Bode Plot of $G_{id}(s)$ in the next section. PI control is a robust technique, and it can work in a range of OPs. The one QOP based on which the controller is designed should be chosen properly.

To alleviate the impact of the real RHP zero, it should be moved away from the imaginary axis and thus should have a large value. In other words, the system performs better with a larger RHP zero. L is the inductance, and it will not change once the converter is designed. The DC values V_o, D, I_L, and R_o can vary at different OPs in different scenarios. Thus, first, L should be small to have a relatively large RHP zero according to (3.10). And QOP should represent the worst-case scenario

with the smallest RHP zero after L is already defined. The smallest RHP zero is obtained either with the minimum V_o, maximum D and maximum I_L, or with the minimum R_o and maximum D. That represents the scenario with the heaviest load and the largest voltage gain k_{ioL}.

$L = 2.54$mH calculated based on $2\%I_{L_max} = 0.26$A as mentioned above. Set $L = 2$mH to get a maximum current ripple $2.5\%I_{L_max} = 0.33$A.

The resistance of the heaviest load for each ES unit is twice that for two ES units: the total minimum resistance $R_{o\_min} = 4.8\Omega$ and $R_{o\_QOP} = 2R_{o\_min} = 9.6\Omega$ for each ES unit. $D_{max} = 0.621$, which is obtained when $v_o = V_{o_max} = 52.8$V and $v_{ES} = V_{ES_L} = 20$V at its lowest SoC.

In the Boost mode, where the ES unit is supplying power, $I_{o\_ES}{}^* > 0$, and $v_o < V_{nl}$ at steady state in primary control. If secondary control is considered, $v_o = V_{nl} = 48$V due to voltage regulation. And if $v_o \neq V_{nl}$ in secondary control, it happens only when reaching the upper boundary of δv, and v_o should still be smaller than V_{nl}. In summary, $v_o \leq V_{nl}$ in the Boost mode. Thus, the maximum duty cycle in Boost mode $D_{QOP} = 0.583$ where $V_{o_OP} = 48$V, and $V_{ES_OP} = 20$V.

Thus, $I_{o\_ES\_QOP} = \frac{V_{o\_QOP}}{R_{o\_QOP}} = 5A$, $k_{ioL\_OP} = \frac{1}{1-D_{QOP}} = 2.4$, and $I_{L\_QOP} = \frac{I_{o\_ES\_QOP}}{(1-D_{QOP})} = 12A$.

RHP zero $Z_{RHP} = \frac{R_o(1-D)^2}{L} = 833$rad/s.

C). Output capacitor C_o

A conventional dual-loop control is shown in Fig 3.3, not used in this thesis. In general, A PI controller $G_{cv}(s)$ should be designed using Bode Plots. The voltage is thus stable and insensitive to the perturbations of load and voltage of the ES unit due to a large loop gain. And v_o can stabilize with a proper settling time and an overshoot due to the phase margin. Also, PI control can have a zero $\tilde{e}_v$ at steady state.

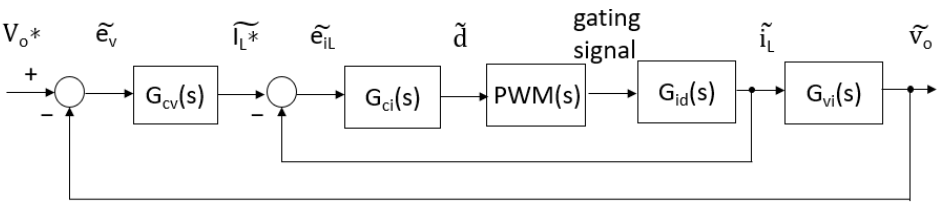

Fig 3.3 Control diagram of conventional dual-loop control

However, according to Fig. 3.2.a), the used primary control of an ES unit has a different dual loop: an inner-current loop and an outer-voltage loop with a constant proportional voltage controller of $\frac{K_{ioL}}{R_{ds\_ES}}$. Due to the gain $\frac{K_{ioL}}{R_{ds\_ES}}$, the primary control has a steady-state error, i.e., $\tilde{e}_v \neq 0$. It is also because v_o is always smaller than $\delta v + V_{nl}$ in the droop region.

Also, given an arbitrary gain instead of a PI controller, the stability of the voltage and the transient characteristics cannot be guaranteed. A proper C_o can be selected for the plant $G_{vi}(s)$ to make sure the voltage v_o can be stabilized as well as obtaining a proper settling time. Since the bandwidth of the inner current loop is relatively high, its closed loop can be approximately seen as a unity gain.

The simplified open-loop TF of primary control is

$$G_{ol\_pri}(s) = \frac{K_{ioL}}{R_{ds\_ES}} G_{vi}(s) = \frac{K_{ioL}[-\frac{L}{(1-D)}s+R_o(1-D)]}{R_{ds\_ES}(R_oC_os+2)}. \tag{3.11}$$

The simplified closed-loop TF from $\tilde{\delta v}$ to $\tilde{v}_o$ is

$$G_{vdv}(s) = \frac{G_{ol\_pri}(s)}{1+G_{ol\_pri}(s)} = \frac{\frac{K_{ioL}}{R_{ds\_ES}}[-\frac{L}{(1-D)}s+R_o(1-D)]}{(R_oC_o-\frac{L}{(1-D)}\frac{K_{ioL}}{R_{ds\_ES}})s+2+R_o(1-D)\frac{K_{ioL}}{R_{ds\_ES}}}. \tag{3.12}$$

To ensure a stable response, the pole of $G_{vdv}(s)$ must be negative, and a minimum C_o can be calculated. Use the parameters in Table 3-1.

Its root is

$$s = -\frac{2+R_o(1-D)\frac{K_{ioL}}{R_{ds\_ES}}}{R_oC_o-\frac{L}{(1-D)}\frac{K_{ioL}}{R_{ds\_ES}}}. \tag{3.13}$$

$$C_o > \frac{\frac{L}{(1-D)}\frac{K_{ioL}}{R_{ds\_ES}}}{R_o} = 2.5mF. \tag{3.14}$$

The primary loop is a first-order system in (3.11) and (3.12). For a standard first-order system, the characteristic equation $s\tau + 1 = 0$. The settling time $t_{set} = 3\tau$ considering 95% of the final value. Although the primary control is not standard. It can still be used to approximate the relationship, $t_{set} = 3\tau = 3\frac{R_oC_o-\frac{L}{(1-D)}\frac{K_{ioL}}{R_{ds\_ES}}}{2+R_o(1-D)\frac{K_{ioL}}{R_{ds\_ES}}}$. Thus,

$$C_o = \frac{1}{R_o}\{\frac{[2+R_o(1-D)\frac{K_{ioL}}{R_{ds\_ES}}]t_{set}}{3} + \frac{L}{(1-D)}\frac{K_{ioL}}{R_{ds\_ES}}\}. \quad (3.15)$$

The smaller C_o is, the smaller t_{set} is. $t_{set} \leq 5$ ms. $C_o \leq 6.32$mF with $L = 2$mH. Set $C_o = 6$mF.

Table 3.1 Parameters of Class C converter at QOP

Parameter	Symbol	Value	Unit
Output voltage	V_{o_QOP}	48	V
Voltage of ES unit	V_{ES_QOP}	20	V
Load	R_{o_QOP}	9.6	Ω
Output current	$I_{o\_ES\_QOP}$	5	A
Inductor current	I_{L_QOP}	12	A
Duty Cycle	D_{QOP}	0.583	1
Voltage gain/current ratio	K_{ioL_QOP}	2.4	1
Output capacitor	C_o	6	mF
Inductor	L	2	mH

Table 3.2 TFs of Class C converter

Name	TF	Zero	Pole
$G_{id}(s)$	$\frac{C_o V_o s + 2\frac{V_o}{R_o}}{LCs^2 + \frac{L}{R_o}s + (1-D)^2}$	$-\frac{2}{R_o C_o}$	
$G_{vd}(s)$	$\frac{-L\frac{V_o}{R_o(1-D)}s + V_o(1-D)}{LC_o s^2 + \frac{L}{R_o}s + (1-D)^2}$	$\frac{R_o(1-D)^2}{L}$	
$G_{vi}(s)$	$\frac{-\frac{L}{(1-D)}s + R_o(1-D)}{R_o C_o s + 2}$	$\frac{R_o(1-D)^2}{L}$	
$G_{ol\_pri}(s)$	$\frac{K_{ioL}[-\frac{L}{(1-D)}s + R_o(1-D)]}{R_{ds\_ES}(R_o C_o s + 2)}$	$\frac{R_o(1-D)^2}{L}$	
$G_{vdv}(s)$	$\frac{\frac{K_{ioL}}{R_{ds\_ES}}[-\frac{L}{(1-D)}s + R_o(1-D)]}{(R_o C_o - \frac{L}{(1-D)}\frac{K_{ioL}}{R_{ds\_ES}})s + 2 + R_o(1-D)\frac{K_{ioL}}{R_{ds\_ES}}}$	$\frac{R_o(1-D)^2}{L}$	$-\frac{2 + R_o(1-D)\frac{K_{ioL}}{R_{ds\_ES}}}{R_o C_o - \frac{L}{(1-D)}\frac{K_{ioL}}{R_{ds\_ES}}}$

It is noted that the RHP zero is inherited in Table 3.2.

The closed loop $G_{vdv}(s)$ has a steady-state error of 0.091 in the step response, as shown below. The settling time t_{set}= 5.97ms, close to the set value of 5ms. There is an undershoot of -0.7 at the beginning due to the RHP zero. It seems very large. However, the bus voltage can never start from 0, and it will always be charged to the nominal value before the start of the control system. Thus, the large undershoot will be avoided.

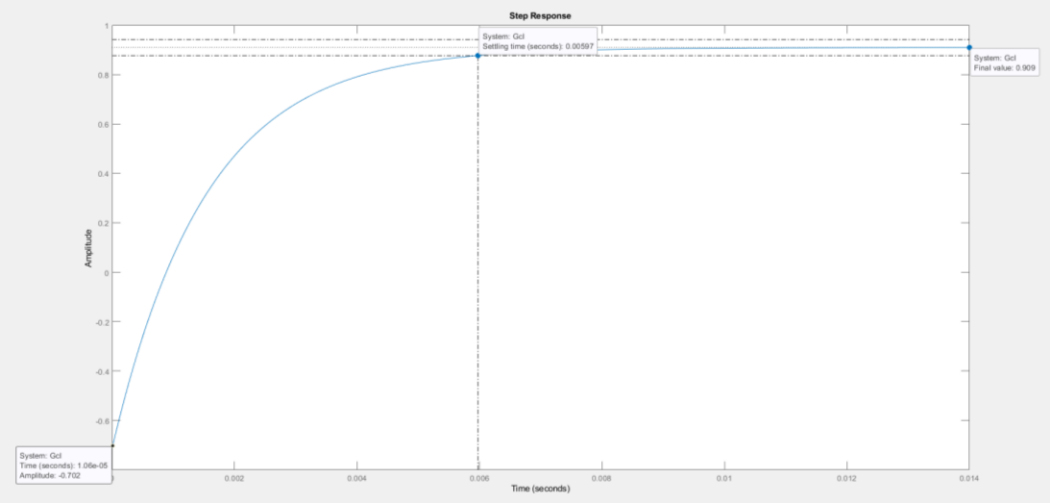

Fig 3.4 Step response of simplified closed loop of primary control $G_{vdv}(s)$ at QOP

Because of the RHP zero, it is a non-minimum phase system. Use the Nyquist plot to verify its stability, as shown in Fig 3.5. Apparently, the closed loop of primary control is stable at QOP.

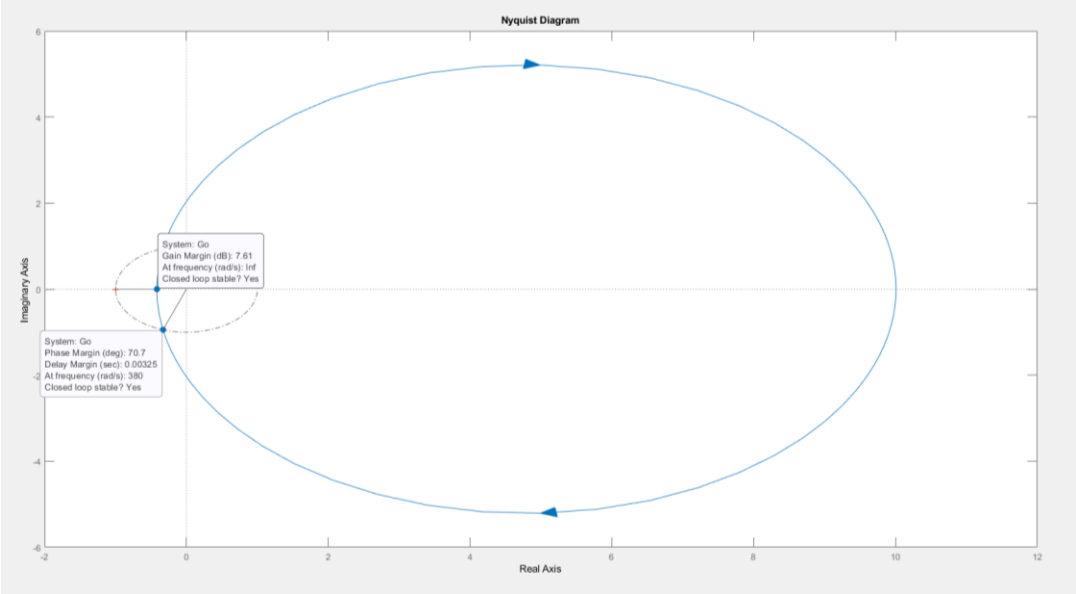

Fig 3.5 Nyquist plot of simplified open-loop TF $G_{ol\_pri}(s)$ at QOP

D). Explanation of a larger C_o

It is noted that C_o calculated here is much larger than 146μF in Section 3.1.3.

A larger C_o is necessary due to three factors: uncontrollable outer-voltage loop in primary control; the RHP zero in Boost mode of the Class C converter; droop control.

Unlike voltage-mode droop control, the outer voltage loop in current-mode droop control does not have a PI controller to stabilize the bus voltage. It only has a gain of $\frac{K_{ioL}}{R_{ds\_ES}}$ as a proportional controller. To ensure the stability, the minimum C_o of 2.5mF is given in (3.14).

The RHP zero in the Boost mode comes from the topology of the Class C converter. If v_o is to be increased, it must decrease first, having an undershoot. Because the inductor needs charging first for a relatively long time, the output capacitor will continue discharging, leading to a decreasing bus voltage. To some extent, droop control aggravates this trend. On the droop line, I_{o_ES}* increases with a smaller voltage. That will again increase the reference of inductor current and prolong the charge time of the inductor. It is a vicious cycle. And the bus voltage keeps decreasing and eventually becomes unstable. A slow response is key to solving the issue of RHP zero. The settling time is thus set to be 5ms in (3.15) and gets 5.97ms in the step response at QOP.

On the other hand, the voltage range in the entire droop region for an ES unit is 4.8V (0.1pu). And C_o is calculated as 146μF based on an acceptable voltage ripple of 1.06V. So, the resolution of the voltage for droop control is 4.8÷1.06 = 22.1%. The variation of the voltage in one switching cycle is too large for droop control. The ripple needs significantly reducing. A large C_o can help reduce the variation of the voltage. The maximum voltage ripple is $0.026V$ with the new C_o, and the resolution becomes 0.54%.

3.3 Design of Inner-current Controller

The control diagram is as below. PWM(s) includes a delay of one switching cycle T_{SW} in digital control. And sampling frequency is equal to the switching frequency f_{sw}= 20kHz.

$$PWM(s) = e^{-sTsw} \tag{3.16}$$

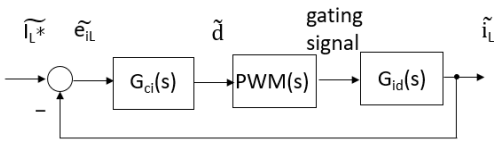

Fig 3.6 Control diagram of inner-current loop

Fig 3.7 shows the Bode Plot of $G_{id}(s)$, based on which a current PI type II controller $G_{ci}(s)$ is designed using the design method of K-factor.

$$G_{ci}(s) = K_{ci}\frac{(1+s\tau_{ci})}{s\tau_{ci}(1+sT_{p\_ci})} \tag{3.17}$$

$K_{ci} = 0.262, \tau_{ci} = 1.514ms,$ and $T_{p\_ci} = 16.726\mu s.$

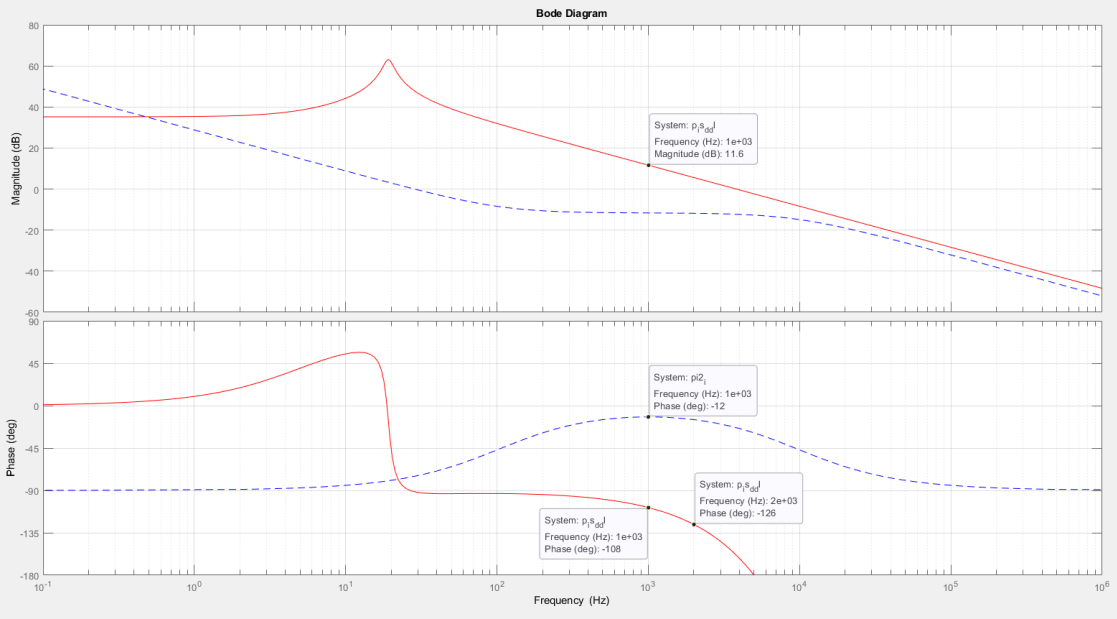

Fig 3.7 Bode plots of $G_{id}(s)$ (in red) and $G_{ci}(s)$ (in blue dash)

It is noted that the phase of $G_{id}(s)$ decreases significantly from 1kHz due to the delay in PWM, where phase $\Phi = -108°$ at 1kHz and $\Phi = -126°$ at 2kHz. A PI type II controller can only decrease the phase at the cross-over frequency of the inner-current loop f_{x_i}. Thus, set $f_{x\_i} = 1\text{kHz} = \frac{f_{sw}}{20}$. Therefore, the phase margin of the inner compensated loop TF $G_{ol\_i}(s)$: $PM_{\_i} = 60°$ at f_{x_i}, as shown in Fig 3.8. The slopes of the gain plot of $G_{ol\_i}(s)$ are -20dB/dec in the low-frequency range and around f_{x_i}, and -40dB/dec in the high-frequency range.

For a second-order system, damping ration $\xi = 0.1PM = 0.6$, corresponding to a percentage of overshoot (PO) of 10%. Although the inner current loop is a high-order system, it can be seen as an equivalent second-order system.

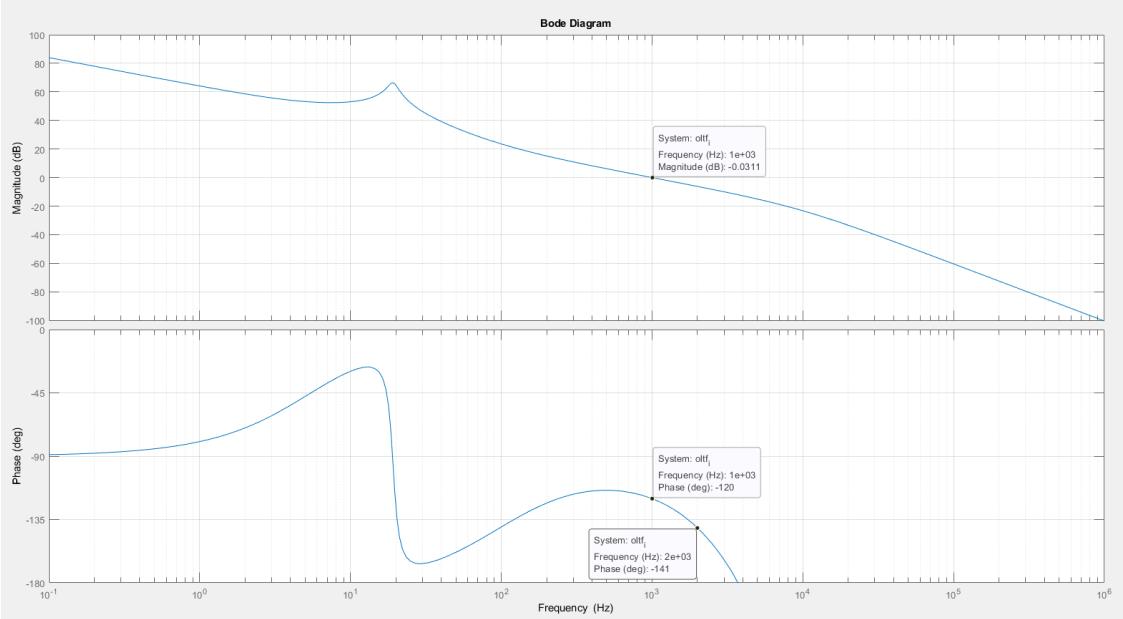

Fig 3.8 Bode plots of open inner current loop

The step response is as below. There is a delay of one switching cycle $T_{SW} = 50\mu s$ at the beginning. Settling time $t_{set\_i} = 2.5ms$. The percentage of overshoot $PO = 10.6\%$, closed to 10%, corresponding to PM of 60°. steady-state error $e_{ss} = 0$.

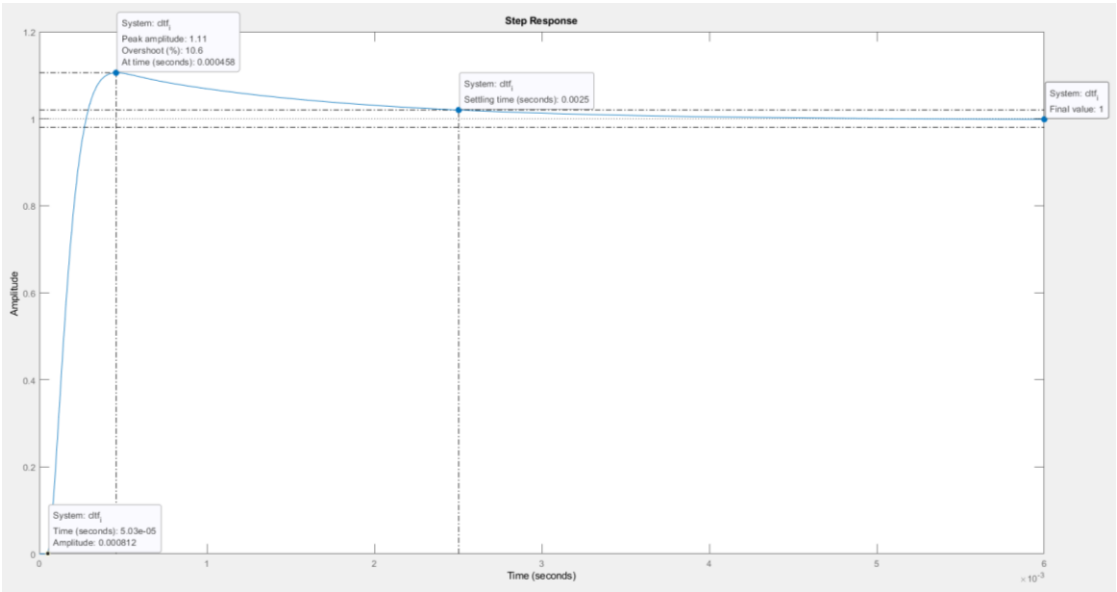

Fig 3.9 Step response of closed inner current loop

3.4 Step Response of Primary Control

3.4.1 Step response of primary control considering secondary control in MATLAB

The stability of the bus voltage in primary control should be tested with the existence of secondary control with a non-zero $\tilde{\delta v}$, as shown in Fig 3.10. This is used to test the internal stability in secondary control. The test will include the closed inner current loop and will not include the secondary controller $G_{cv}(s)$.

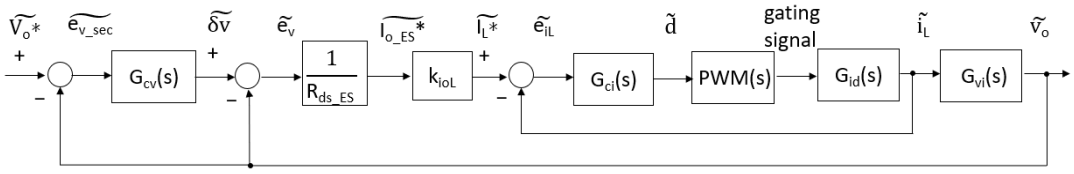

Fig 3.10 Secondary control diagram of an ES unit

The tested closed loop of primary control is from $\tilde{\delta v}$ to $\tilde{v}_o$ in MATLAB, as shown in Fig 3.2.a).

The primary control should be stable at QOP with a step input $\tilde{\delta v}$ using PI controller $G_{ci}(s)$. When away from QOP, the plant TFs $G_{id}(s)$ and $G_{vi}(s)$ will change according to the DC values of V_{ES}, V_o, and R_o (D and I_L) in simulation and the real world. However, the system is still supposed to perform well with the designed current controller $G_{ci}(s)$. As mentioned before, the chosen QOP should be the worst-case scenario in terms of stability. If the system is tested stable with $G_{id}(s)$ and $G_{vi}(s)$ at QOP, the system should also be stable at other possible operating points with variable DC values of the parameters. Thus, $G_{ci}(s)$ can be verified as well designed.

A). at QOP

The step response of the closed primary control is as below. The settling time is 6.48ms. The steady-state value is 0.909, and $\tilde{e}_v = 0.091$. There is an undershoot of -0.51. The transient characteristics are close to those in Fig 3.4, where the closed inner current loop is seen as a unity gain. In summary, the above test verifies the stability of the system in the worst-case scenario, where the load demand is the largest, to a step input $\tilde{\delta v}$.

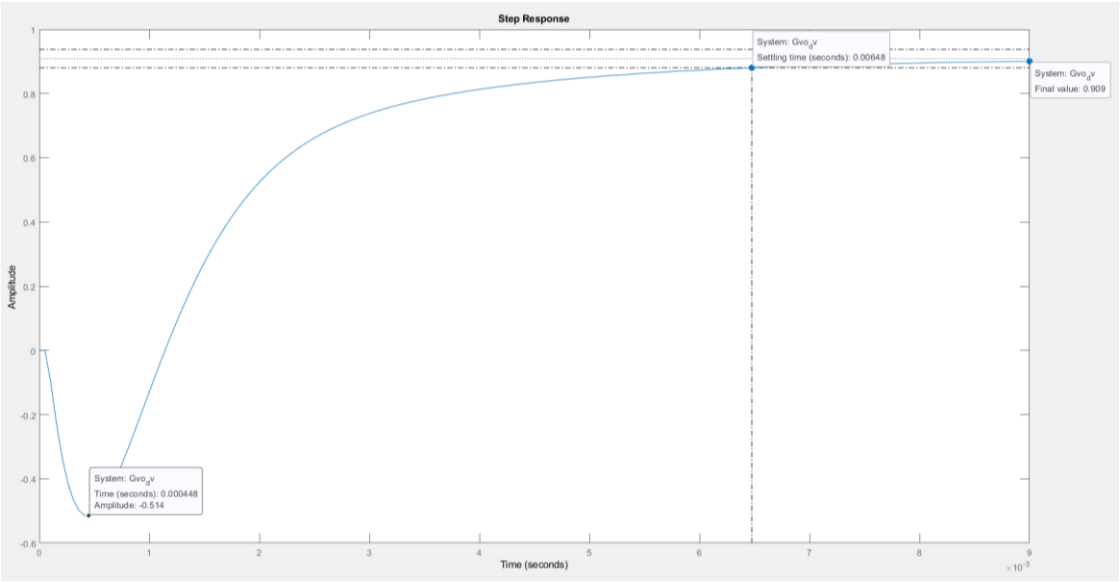

Fig 3.11 Step response of primary control with step input $\tilde{\delta v}$

B). away from QOP with R_o= 12Ω

The step response is as below. It is noted that the undershoot is smaller, -0.36, and thus the impact of RHP Zero is smaller with smaller load demand. The settling time is a bit longer, 7.42ms. The steady-state error is smaller, 0.072.

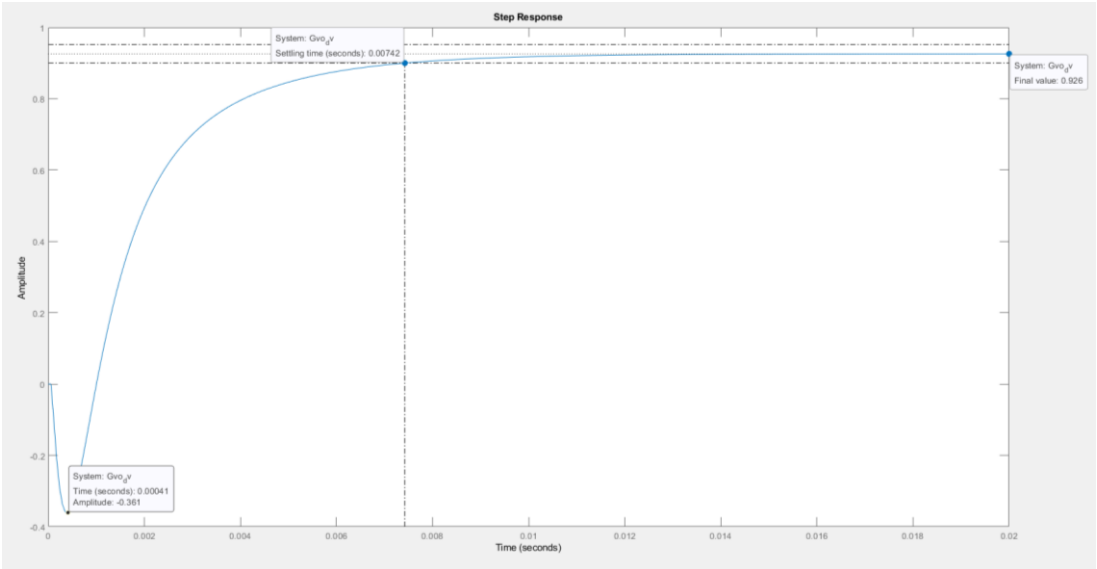

Fig 3.12 Step response of primary control with step input $\tilde{\delta v}$ and smaller load demand

3.4.2 Step response of primary control without secondary control in SIMULINK

The stability of the primary control should also be tested without the secondary control signal. If secondary control does not exist, for instance communication fails, the outside input for the primary control $\tilde{\delta}v = 0$. On the other hand, the low-bandwidth communication among sensors, the primary controller, and the secondary controller might take some time to update $\tilde{\delta}v$. Thus, to the primary control loop, the secondary controller $G_{cv}(s)$ can also be regarded as not existing after sending a $\tilde{\delta}v$ before the next coming cycle.

Also, as mentioned before, v_o is insensitive to load variation in a conventional control method, as shown in Fig 3.3, due to the voltage PI controller not used in this thesis. Thus, a test from the load variation to $\tilde{v}_o$ is not necessary. However, v_o is sensitive to load variation in droop control, and droop control intentionally yields voltage variation. Thus, the performance of $\tilde{v}_o$ based on a change in load should be tested.

For primary control only, the variation of load can be regarded as an input, and it will change the operation of an ES unit and the Nanogrid. The change of the voltage of ES unit will be very slow and thus not tested here.

In the small-signaling model, the load/output current $I_{R_o} + \tilde{\imath}_{R_o} = \frac{V_o + \tilde{v}_o}{R_o + \tilde{r}_o}$. Apparently, it is nonlinear if R_o is regarded as the input at the denominator. Therefore, $\tilde{\imath}_{R_o}$ is the input and represents the variation of the output current and thus the variation of the load. The new control diagram is shown in Fig 3.13. The designed current control $G_{ci}(s)$ does not change in the test. It is more convenient to do the test in SIMULINK.

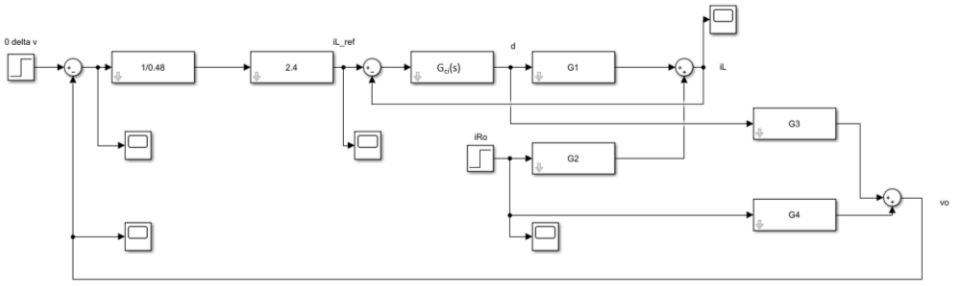

Fig 3.13 Control diagram of primary control with step input $\tilde{\imath}_{R_o}$ in SIMULINK

The new plant model can be obtained as below in (3.18), considering the delay in the PWM module. $G_1(s)$ and $G_3(s)$ are the TFs from control to outputs and $G_2(s)$ and $G_4(s)$ are from the load perturbation to the outputs.

$$i_L(s) = G_1(s)d(s) + G_2(s)i_{R_o}(s) = \frac{C_oV_os+I_L(1-D)}{LCs^2+(1-D)^2}e^{-sT_{sw}}d(s) + \frac{(1-D)}{LCs^2+(1-D)^2}i_{R_o}(s);$$

$$v_o(s) = G_3(s)d(s) + G_4(s)i_{R_o}(s) = \frac{-LI_Ls+V_o(1-D)}{LCs^2+(1-D)^2}e^{-sT_{sw}}d(s) + \frac{-Ls}{LCs^2+(1-D)^2}i_{R_o}(s). \quad (3.18)$$

A). at QOP

With a unit step in $\tilde{\imath}_{R_o}$, due to an increase in load demand, the inductor current is expected to be raised. $\tilde{v}_o$ will decrease according to droop control. The step response of $\tilde{\imath}_L$ and $\tilde{v}_o$ are shown below with a step input of $\tilde{\imath}_{R_o}$. $\tilde{\imath}_L$ increases and $\tilde{v}_o$ decreases, and both can be stabilized in the responses. The settling times for both are around 5ms. The steady-state values of $\tilde{\imath}_L$ and $\tilde{v}_o$ are 2.284A and -4.568V, respectively.

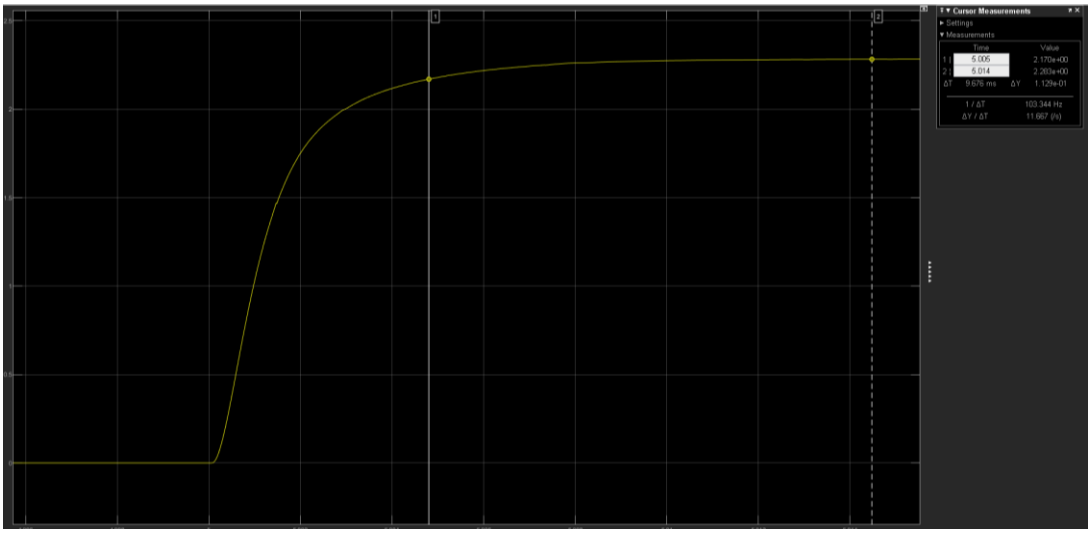

Fig 3.14.a) Step response of $\tilde{\imath}_L$ in primary control with step input $\tilde{\imath}_{R_o}$ in SIMULINK

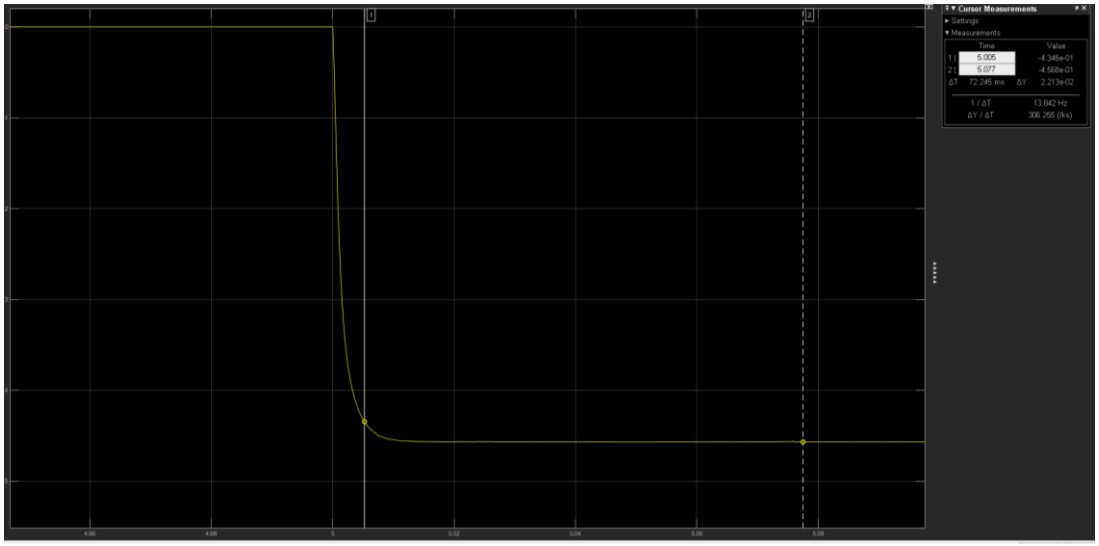

Fig 3.14.b) Step response of $\tilde{v}_o$ in primary control with step input $\tilde{\imath}_{R_o}$ in SIMULINK

It is expected that v_o decreases by 0.48V if i_{Ro} increase by 1A, since $v_o = -i_o R_{ds\_ES} + V_{nl} + \delta v$ in droop control. v_o decreases by 0.457V when i_{R_o}increases by 1A in the test. It is because the inductor current is controlled instead of the output current leading to the inaccuracy of power-sharing. In simulation and real world, a dynamic gain k_{ioL} can be used to solve this problem.

B). away from QOP with $R_o = 12\Omega$

The system can still stabilize with a settling time of 6ms, as shown below. The steady-state values of $\tilde{\imath}_L$ and $\tilde{v}_o$ are 2.306A and -0.461V, respectively.

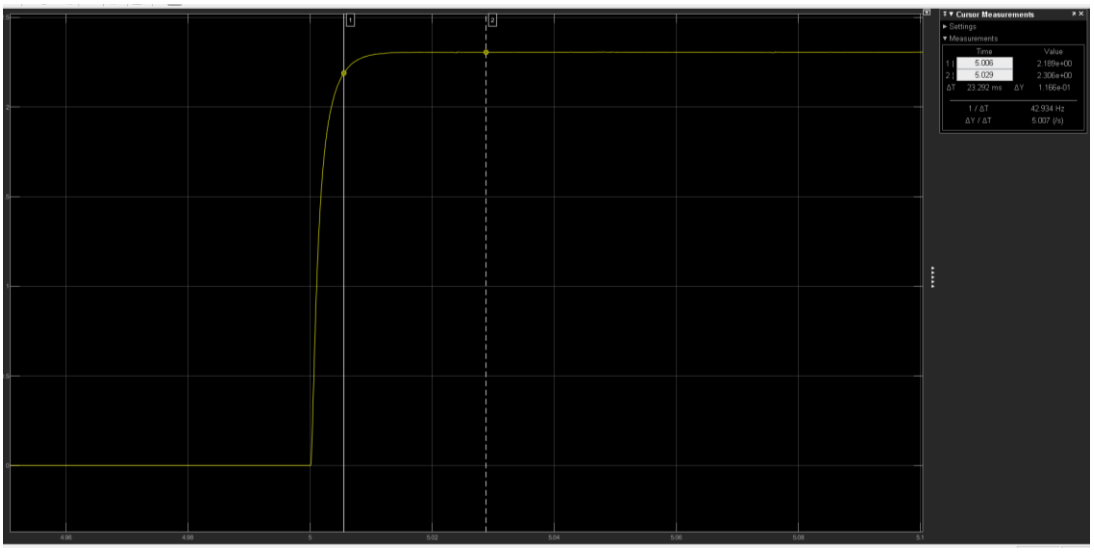

Fig 3.15.a) step response of $\tilde{\imath}_L$ in primary control with step input $\tilde{\imath}_{R_o}$ and smaller load demand in SIMULINK

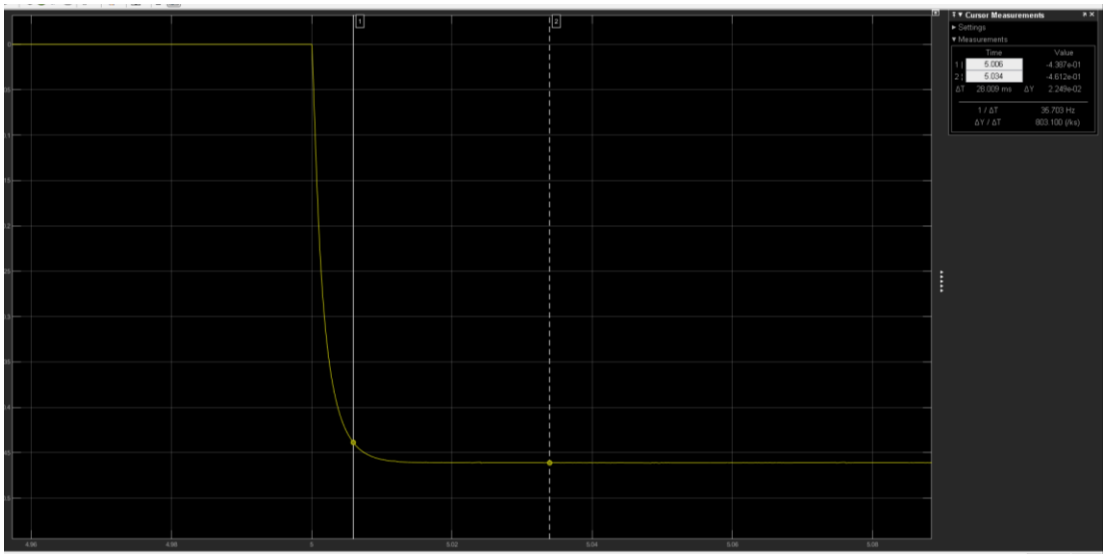

Fig 3.15.b) Step response of $\tilde{v}_o$ in primary control with step input $\tilde{\imath}_{R_o}$ and smaller load demand in SIMULINK

In summary, the bus voltage v_o can stabilize in primary control with or without secondary control.

3.5 Accurate Power-sharing: Dynamic Current Ratio k_{ioL}

As beforementioned, one objective of droop control of ES units is to achieve accurate power-sharing, where the output power $P_{ES} = v_o i_{o\_ES} = v_o \, {I_{o\_ES}}^*$. However, due to the topology of the Class C converter, its output current cannot be controlled directly, and the input/inductor current i_L is controlled. In the control diagram and step response test, the current ratio between i_L and i_o at QOP, $K_{ioL\_OP} = \frac{{I_L}^*}{{I_{o\_ES}}^*} = 2.5$. Therefore, $P_{ES} = \frac{1}{K_{ioL\_OP}} v_o i_L \neq v_o \, {I_{o\_ES}}^*$ if away from QOP. Power cannot be shared as desired.

In simulation and real world, a dynamic gain can be calculated based on the measurements of the output voltage (v_o) and the input voltage (v_{ES}) of the converter, and $k_{ioL} = \frac{v_o}{v_{ES}}$. $i_L = {I_L}^* = k_{ioL} \, {I_{o\_ES}}^*$, and thus $P_{ES} = v_o i_o = v_o \frac{1}{k_{ioL}} i_L = v_o \, {I_{o\_ES}}^*$ in primary control at steady state. The dynamic gain can be a factor multiplied after ${I_{o\_ES}}^*$, as shown below.

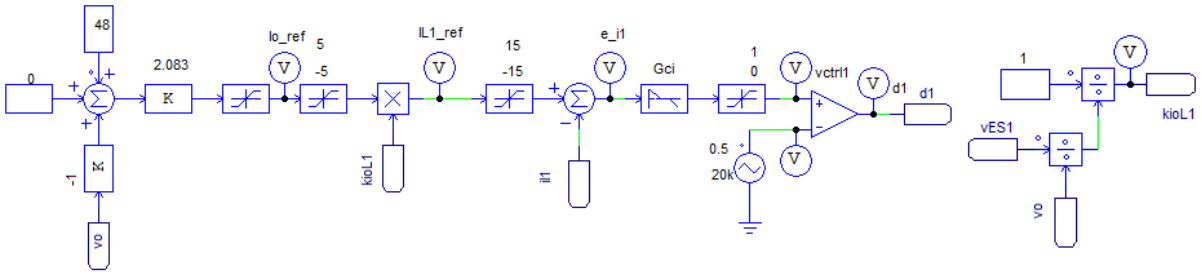

Fig 3.16 Primary control diagram of an ES unit including k_{ioL} in PSIM

Chapter 4 Design of Secondary Control for Isolated DC Nanogrid

Secondary control composes of voltage regulation and State of Charge (SoC) control. Voltage regulation maintains the bus voltage at its nominal value for power quality at steady state. SoC control avoids ES units overcharging and deep discharging, and it can also balance the SoC of multiple ES units letting the suitable ES unit supply or absorb more power. These two control methods are both employed based on primary droop control.

4.1 Voltage Regulation

4.1.1 discusses the scheme of voltage regulation by shifting the original droop curve in primary control. 4.1.2 introduces a model of the proposed isolated DC Nanogrid, based on which 4.1.3 discusses the design of the secondary controller. 4.1.4 compares the model used in 4.1.2 and the original one-ES unit model. The original model is verified to better describe the Nanogrid in simulations.

4.1.1 Droop based voltage regulation for an ES unit

Fig 4.1 shows the original droop curve of an ES unit in primary control in black. Due to voltage regulation on the secondary control level, its control signal δv shifts the original droop curve. The updated curves are in blue and orange. Voltage regulation maintains the bus/load voltage v_o at V_{nl} at steady state, such as Point A, C, F, 1, and 2. Also, the modified curves are clamped by the limit of $[-I_{ES\_max}, I_{ES\_max}]$.

If the ES unit is discharging, the reference of the output current $I_o{}^*$ is positive, and thus the Operating Point (OP) is on the RHP. Voltages on the RHP are smaller than V_{nl} in original droop control, the curve is then shifted upwards with a positive δv. The ES unit supplies more power, and v_o is raised to V_{nl}. Therefore, if the ES unit is discharging, the OP must be on the RHP, and δv must be positive 0.

On the other hand, $\delta v > 0$ in voltage regulation means that v_o is to be increased and moved closer to V_{nl} as the curve is shifted up. It only happens to the OPs on the RHP where $v_o < V_{nl}$ in original droop control. And it will never happen to the OPs on the Left Half Plane (LHP). Since $v_o > V_{nl}$

in original droop control on the LHP, v_o cannot be increased and moved closer to V_{nl} at the same time, instead if v_o is increased it is moved farther from V_{nl}.

In summary, if the OP is on the RHP, δv must be positive. And if δv is positive, the OP must be on the RHP, and the LHP part of the shifted droop curve is missing. Similarly, if $\delta v < 0$, the RHP part is missing.

And the above rule impacts the voltage range with a certain δv. For instance, the LHP part of the blue line next to Point E is missing. With the current δv, the maximum voltage will be obtained at Point D instead of V_{ES_max}, and the minimum voltage is at Point E larger than V_{ES_min}.

The RHP part of the orange line next to Point H is missing. The maximum voltage is at Point G, smaller than V_{ES_max}, and the minimum voltage is at Point H. The rule of the voltage range applies for steady state and the transient period since it is not always the ideal case that $v_o = V_{nl}$ at steady state. Voltage regulation reaches its maximum capability when δv reaches its either boundary. However, the bus voltage is still closer to V_{nl} than without voltage regulation. It is shown in the simulation results.

Assume that the current OP is at Point A. Then power demand decreases. Along the droop curve, due to parameter values, the output power decreases with an increasing voltage. Before secondary control updates δv, the OP climbs gradually to Point B along the droop curve according to primary control. It is because primary control is much faster than secondary control. Primary control keeps changing the output current reference I_o^* with a varying v_o.

Moreover, the inductor i_L can follow the reference I_L^* very well, and it can be regarded as $i_L = I_L^*$ during the entire period. Assume that the output current i_{o_ES} can also follow its reference I_o^* well through k_{ioL} where $i_{o\_ES} = I_o^*$. In fact, k_{ioL} is not the accurate ratio between i_L and i_o in the transient, and $i_{o\_ES} \neq I_o^*$. For simplicity, make the above assumption.

Thus, the OP can slide along the droop curve due to primary control with an unchanged δv. Then secondary control generates a new smaller δv, and the final OP reaches Point C after sliding along the new droop curve. And $v_o = V_{nl}$ again at steady state.

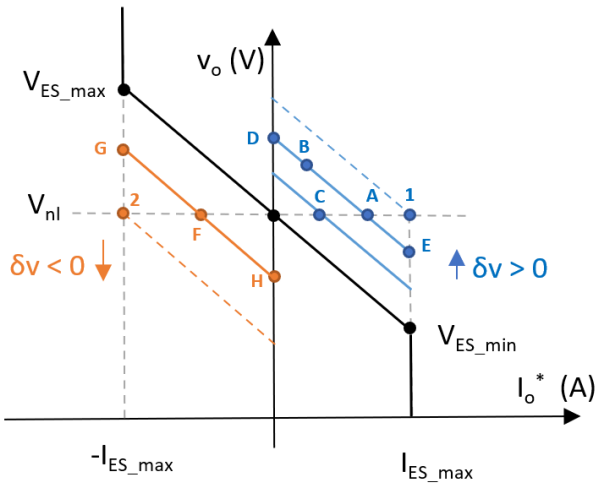

Fig 4.1 Droop based voltage regulation

The ES unit can obtain its rated power at Point 1 at steady state, while the ES unit is discharging and $\delta v > 0$. $P_{ES\_1} = V_{nl} I_{ES\_max}$. And with any δv smaller than the current δv at Point 1, the output power is smaller than the rated power at steady state. To make sure the ES unit can reach its rated power but does not exceed it much, voltage regulation should allow the ES unit to reach slightly above Point 1. Thus,

$$\delta v_{max} \geq V_{nl} - V_{ES\_min}. \tag{4.1}$$

Similarly, Point 2 is the negative rated power point at steady state while the ES unit is charging and $\delta v < 0$. Thus,

$$\delta v_{min} \leq V_{nl} - V_{ES\_max}. \tag{4.2}$$

$$\delta v_{max} \geq 2.4\text{V}, \text{ and } \delta v_{min} \leq -2.4V. \tag{4.3}$$

Set $\delta v \in [-2.5, 2.5]$.

4.1.2 Model of isolated DC Nanogrid

As the beforementioned, the design of primary control of an ES unit only considers one ES unit in the Boost mode based on a worst-case scenario.

When voltage regulation is discussed, the entire DC Nanogrid is considered, including 2 ES units and 1 PV unit. The secondary control is also designed based on the previous worst case in the Boost mode due to the RHP zero. Since the PV unit is supposed to work in the MPPT mode, it generates constant power, and assume its current is also constant. The PV unit can be neglected in modeling

the DC Nanogrid. Furthermore, two ES units generate 480W in total in the worst-case scenario. And the maximum load demand is 480W. Thus, if the PV unit also supplies power, the system is not operating in the worst case. Therefore, the PV unit does not generate power at QOP based on which the primary and secondary controllers are designed, and the PV unit is neglected. Modeling an isolated DC Nanogrid becomes modeling two ES units.

Equivalent model of two ES units

Since the two ES units are identical, two ES units can be combined into one equivalent larger ES unit with changed TFs $G_{id\_eq}(s)$ and $G_{vi\_eq}(s)$ and droop factor $R_{ds\_ES\_eq}$. The control diagram is as below.

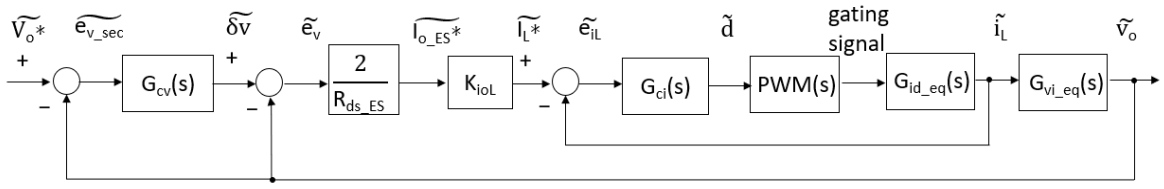

Fig 4.2 Control diagram of voltage regulation for Nanogrid

The TFs in the Boost mode are as below.

$R_{o\_eq} = \frac{R_o}{2} = 4.8\Omega, C_{o\_eq} = 2C_o = 12mF,\ I_{L\_eq} = 2I_L = 24A,$ and $R_{ds\_ES\_eq} = \frac{R_{ds\_ES}}{2} = 0.24.$

$$G_{id\_eq}(s) = \frac{i_L(s)}{d(s)} = \frac{C_o V_o s + 2\frac{V_o}{R_o}}{LC_o s^2 + \frac{L}{R_o}s + \frac{(1-D)^2}{2}}. \quad (4.4)$$

$$G_{vi\_eq}(s) = \frac{v_o(s)}{i_L(s)} = \frac{-\frac{L}{(1-D)}s + \frac{R_o(1-D)}{2}}{R_o C_o s + 2}. \quad (4.5)$$

The equivalent inner current loop is stable, and its Bode plots and step response are the same as those before mentioned, as shown in Fig 4.3 and Fig 4.4. The equivalent closed loop of primary control is stable according to the Nyquist plot, as shown in Fig 4.5.

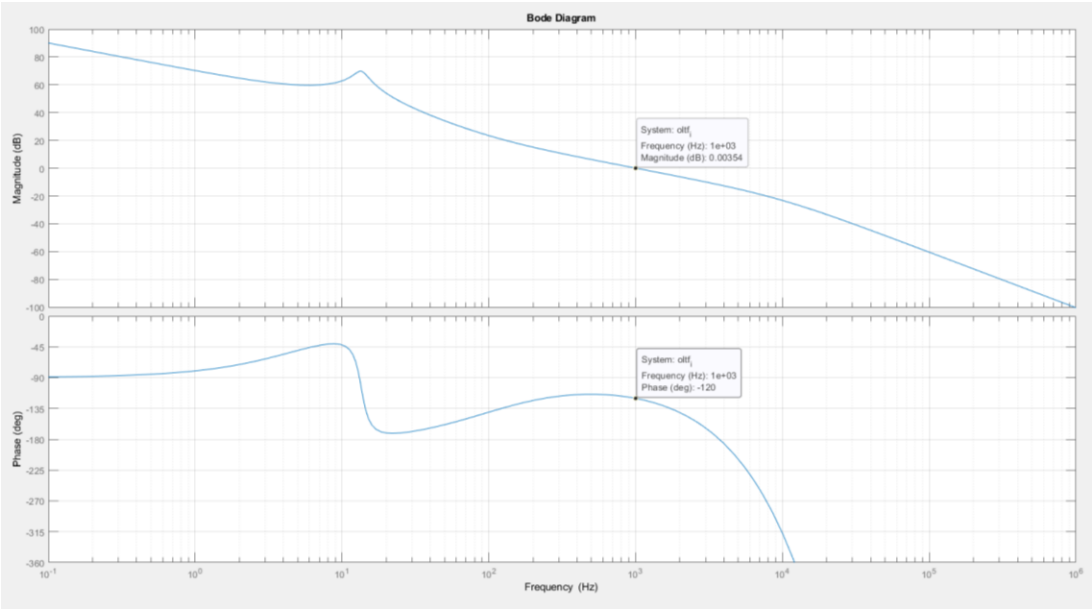

Fig 4.3 Bode plots of equivalent TF $G_{id\_eq}(s)$

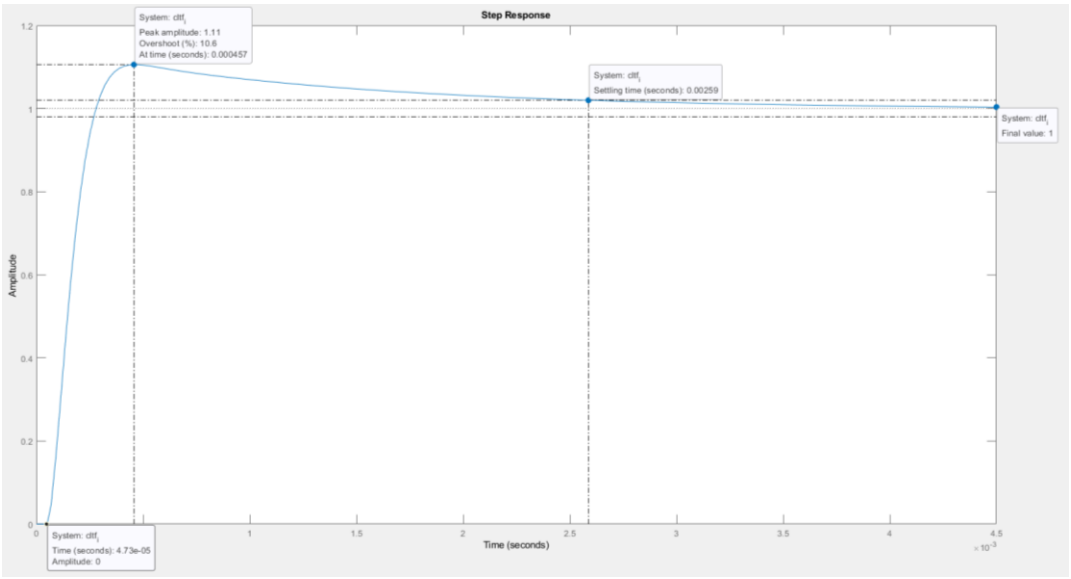

Fig 4.4 Step response of equivalent inner-current loop

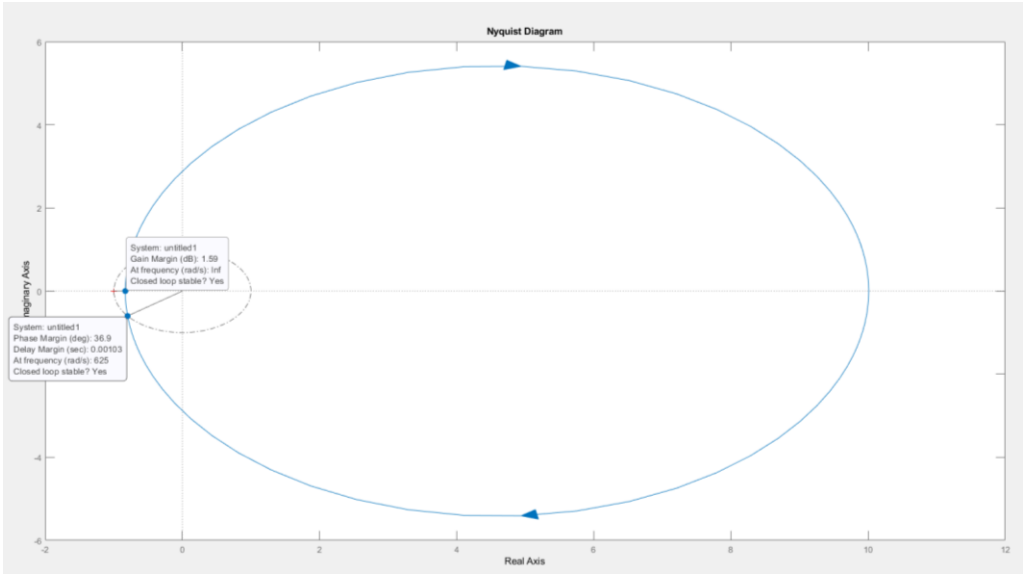

Fig 4.5 Nyquist plot of simplified equivalent open loop of primary control $K_{ioL}R_{ds\_ES\_eq}G_{vi\_eq}(s)$

Note that the RHP zero in $G_{vi\_eq}(s)$ becomes smaller in (4.5). And the step response of primary control is obviously worse now. It is damping with a larger undershoot and an additional large overshoot. The settling time is much longer. Oscillation is mainly due to the larger gain $\frac{2}{R_{ds\_ES}}$.

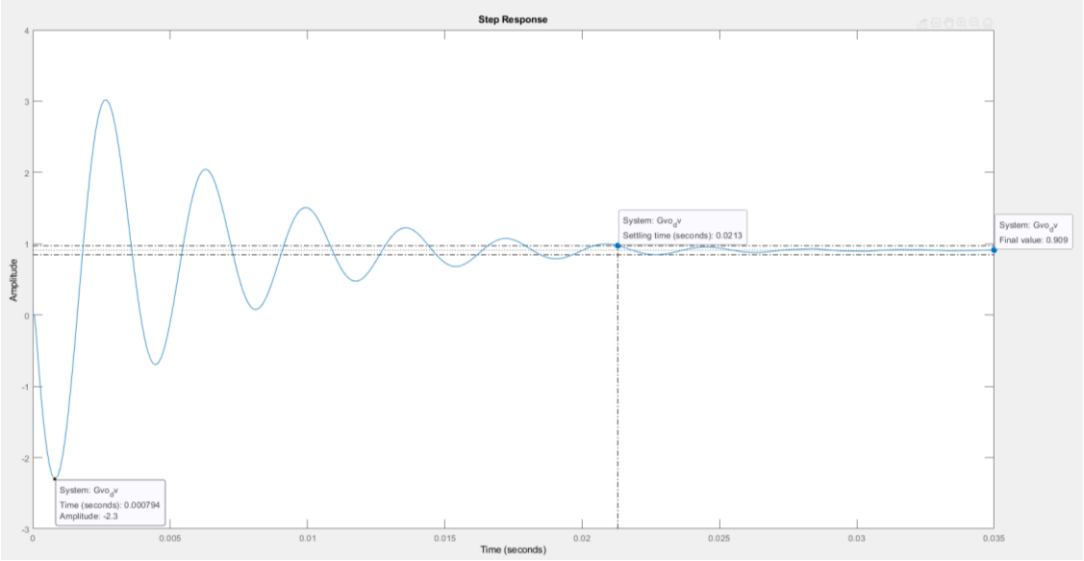

Fig 4.6 Step response of equivalent closed loop of primary control including closed inner-current loop

4.1.3 Design of secondary controller

Fig 4.7 shows the Bode plots. Since the closed loop of primary control has a zero gain in the low-frequency area, an integer is added to get the desired Bode plots. To have a sufficient PM, the cross-over frequency must be smaller than 30Hz. Chose 20Hz and set PM = 60°.

A PI controller is designed using the design method of K-factor where $K_{cv} = 130.317, \tau_{cv} = 45.132ms$. Thus, the secondary controller $G_{cv}(s) = K_{cv}\frac{\tau_{cv}s+1}{\tau_{cv}s^2}$.

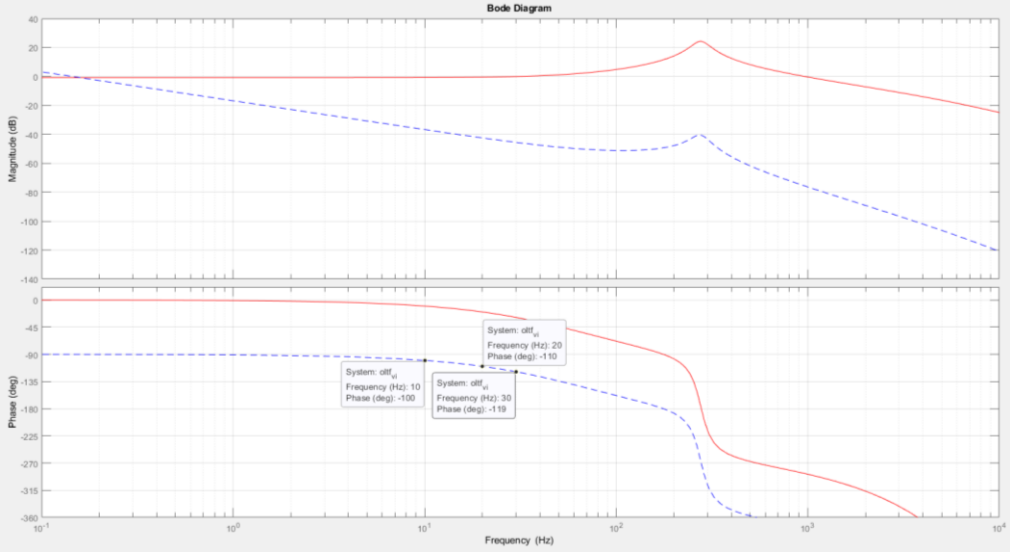

Fig 4.7 Bode plots of closed loop of primary control (in red) and closed loop of primary control in series with an integer (in blue)

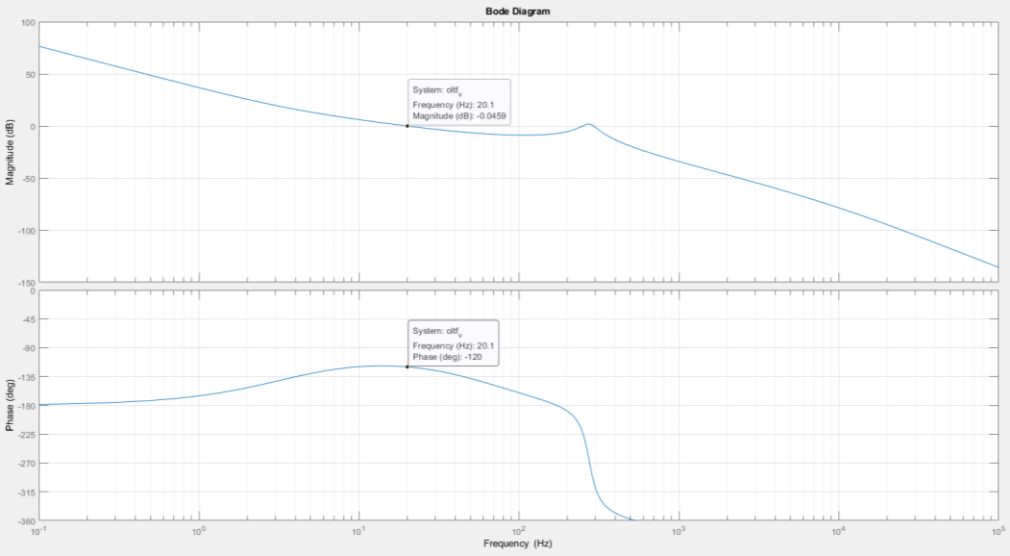

Fig 4.8 Bode plots of open loop of secondary control

Note that, the step response, as shown in Fig 4.9, inherits the dampness from primary control in Fig 4.6 but performs better with a longer settling time of 93.5ms. The undershoot is -34.3%, and the overshoot is 14.4%. There is no steady-state error, i.e., $v_o = V_o^*$ at steady state.

The curve can be smoothed by decreasing the cross-over frequency in the secondary loop. However, there will be a longer settling time and a larger overshoot in that case. Thus, the cross-over frequency is kept at 20Hz.

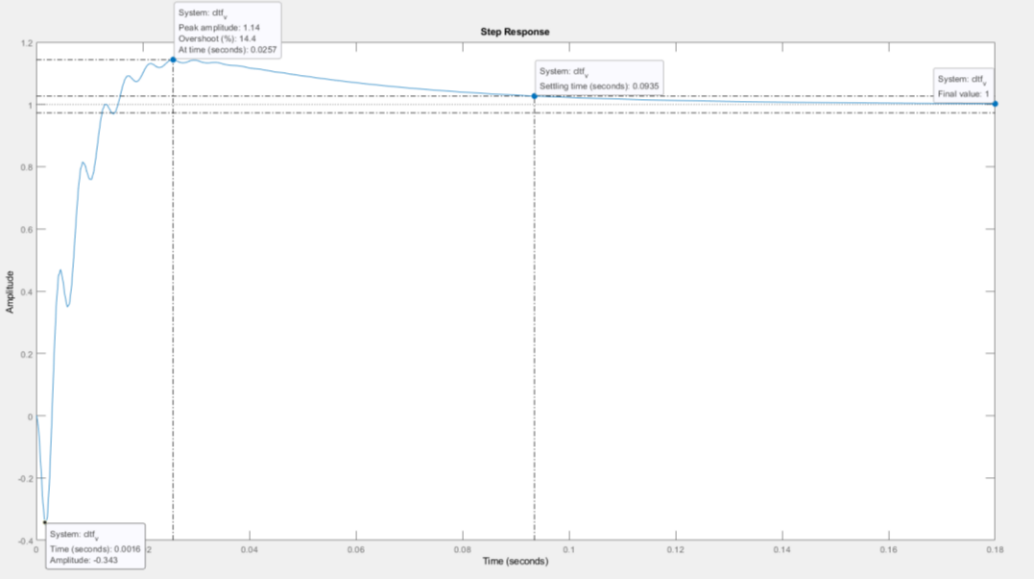

Fig 4.9 Step response of secondary control

4.1.4 Model comparison: original one ES-unit model vs. equivalent one ES-unit model

After designing the secondary controller, the used equivalent model of the Nanogrid can be verified. There are two models: original one ES-unit model, as shown in Fig 3.10; and equivalent one ES-unit model, as shown in Fig 4.2. The former only considers one ES unit, and the latter combines two ES units into one larger ES unit.

A test in simulations in PSIM is used to verify which model can better describe the realistic scenario (two identical ES units). The simulation results are shown below. v_o, i_L, and *delta_v* are the bus voltage, inductor current, and δv, respectively. 1ES_or is for the original one ES unit with circuit parameters R_o, C_o, I_L and R_{ds_ES}. 2ES_ac is for the actual model of two ES units with R_o, C_o, I_L and R_{ds_ES} for each unit, thus load of $\frac{R_o}{2}$ in total. 1ES_eq is for equivalent one ES unit with $R_{o\_eq} = \frac{R_o}{2}$, $C_{o\_eq} = 2C_o$, $I_{L\_eq} = 2I_L$ and $R_{ds\_ES\_eq} = \frac{R_{ds\_ES}}{2}$.

Secondary control is activated. Load R_o jumps initially from 48Ω to 24Ω, 16Ω, 12Ω, 9Ω at time 0.2s, 0.4s, 0.6s, 0.8s for 1ES_or. Load R_o jumps initially from 24Ω to 12 Ω, 8Ω, 6Ω, 4.8Ω at time 0.2s, 0.4s, 0.6s, 0.8s for 2ES_ac and 1ES_eq. The simulation results are shown below.

δv in three cases are overlapping each other neglecting the impact of v_o in the last segment. v_o and i_L are overlapping in 1ES_or and 2ES_ac, respectively. However, note that the transient and steady-state characteristics of 1ES_eq are also very close to those of 2ES_ac. v_o has a bit larger undershoot in 1ES_eq, and the largest difference is 0.15V at 0.6s. But v_o has almost the same settling time in 1ES_eq and 2ES_ac. i_L performs almost the same, only a slightly larger overshoot after 0.6s in 1ES_eq.

Overall, based on the performance, the original one ES-unit model can better describe the actual model of two identical ES units than the equivalent model. However, since the performance of the equivalent model is also close to that of the actual case. It is still valid to use the equivalent model. And it will be convenient, especially when multiple ES units all use the same converter but have different capacities in terms of currents and voltages.

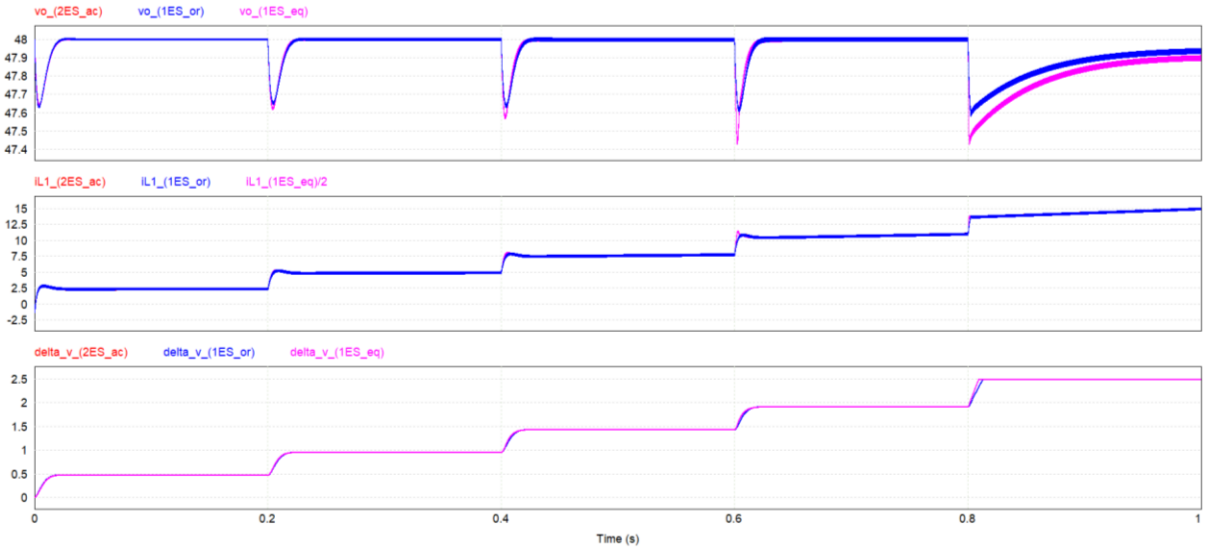

Fig 4.10 Comparison of Nanogrid models using primary control in simulations

The Bode plots of open loop of secondary control for the original one-ES unit are as below. Note that the cross-over frequency is around 20Hz, and PM= 61°, as shown in Fig. 4.11. They are almost the same as those in the equivalent model in Fig 4.8. The difference from the previous Bode plots is that the quality factor Q related to the damping ratio.

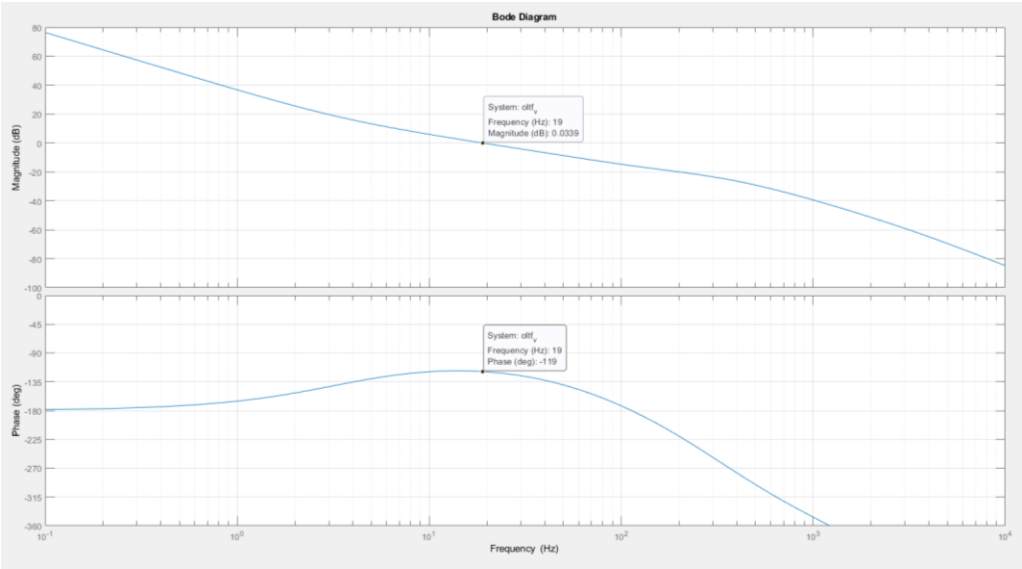

Fig 4.11 Bode plots of open loop of secondary control using original one ES-unit model

Fig 4.12 should be able to describe the actual two ES unit scenario better than Fig. 4.9, based on the comparison of the simulation results. The step responses of the original model and equivalent model have similar overshoot and settling times. However, the original model has a much smaller undershoot and a smoother curve. This characteristic also appears in simulation results.

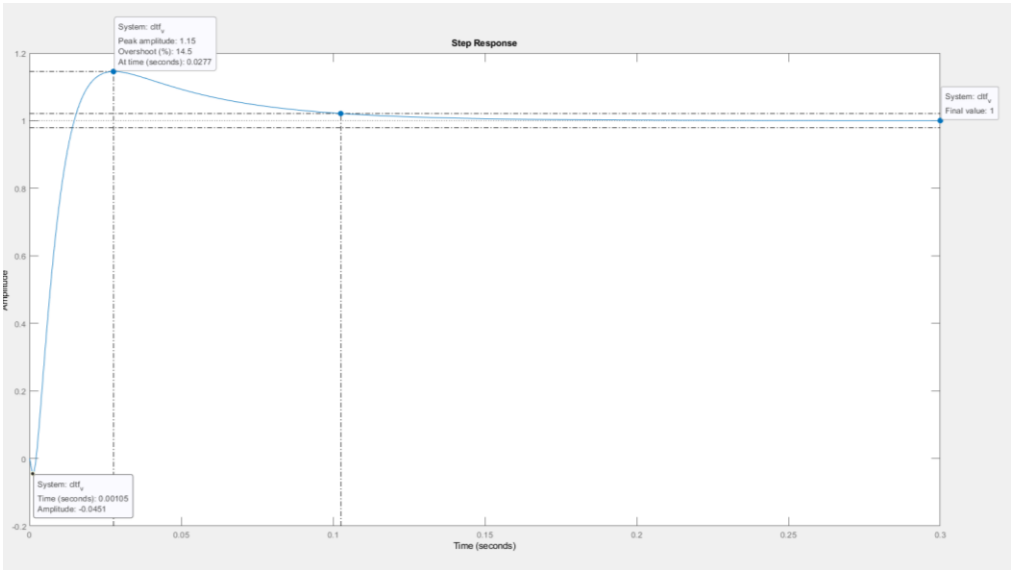

Fig 4.12 Step response of secondary control using original one ES-unit model

4.2 Droop Based SoC Control

In order to prevent damaging ES units and prolong their lifetime, SoC needs control. The goals of SoC control include: 1) stop charging at its upper limit and stop discharging at its lower limit; 2) ES units can collaborate and balance their SoC. SoC control is implemented on the secondary control level. Because the variation of SoC will not be fast, secondary control can handle it well.

Due to current-mode droop control, the reference of the output current I_o^* is generated. Therefore, SoC can be controlled by a current-control method with a SoC factor k_{SoC} [24]. New output current reference:

$$I_o^* = k_{SoC}\frac{-v_o + V_{nl} + \delta v}{R_{ds\_ES}}. \tag{4.6}$$

$$k_{SoC} = \begin{cases} 0, & \text{SoC} < \text{SoCl when Discharging} \\ \frac{SoC - SoC_l}{SoC_{nl} - SoC_l}, & \text{SoCl} < \text{SoC} < \text{SoCnl when Discharging} \\ \frac{SoC_u - SoC}{SoC_u - SoC_{nu}}, & \text{SoCnu} < \text{SoC} < \text{SoCu when Charging} \\ 0, & \text{SoC} > \text{SoCu when Charging} \\ 1, & \text{Otherwise} \end{cases} \tag{4.7}$$

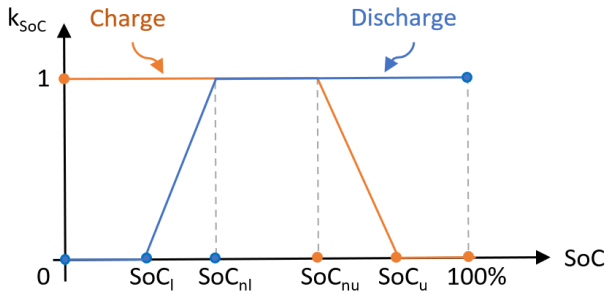

Fig 4.13 Current factor k_{SoC}

According to (4.6), the magnitude of the output current i_o decreases linearly from SoC_{nl} and becomes 0 at SoC_l during discharging. And the magnitude of i_o decreases linearly from SoC_{nu} and becomes 0 at SoC_u during charging. And the power of the ES unit changes along with the current. This method is straightforward and can have the power reach zero and thus stop charging and discharging. Charge and discharge are distinguished, and thus the ES unit can still charge as expected from SoC_{nl} to SoC_l.

SoC control changes the droop factor R_{ds_ES} to $\frac{R_{ds\_ES}}{k_{SoC}}$, as shown in Fig 4.14. Previously, two identical ES units with different SoC both supply current I_0, and $v_o = V_{nl}$ due to voltage regulation. ES unit 2 starts to work in SoC control and reduces its current to I_2 at steady state with a larger slope. The slope of ES unit 1 does not change. It makes up the losses and outputs a larger current I_1 by an increased δv due to voltage regulation. Additionally, $v_o = V_{nl}$ at steady state, and the two ES units have the same δv.

Thus, the ES unit with a larger SoC can supply more power if the other ES unit is in SoC mode. And since it supplies more power, decreasing its SoC faster and thus narrowing the gap in SoC of the two ES units.

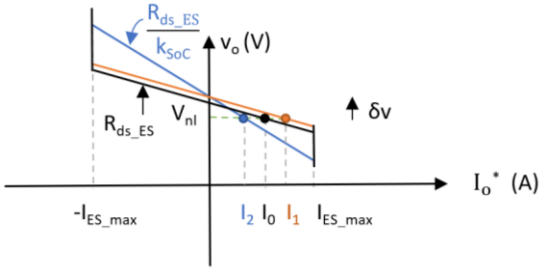

Fig 4.14 Droop based SoC control

Since supercapacitors are used as ES units in this thesis, the evaluation of SoC is as below [38].

$$SoC = \frac{{v_{ES}}^2}{{v_{ES\_max}}^2}. \tag{4.8}$$

Implementation of SoC control in simulation

The control parameters are shown in Table 4.1.

Table 4.1 Parameters in SoC control

Parameter	Symbol	Value	Unit
Lower limit of SoC	SoC_l	39.1	%
Near lower limit of SoC	SoC_{nl}	47.3	%
Near upper limit of SoC	SoC_{uu}	76.6	%
Upper limit of SoC	SoC_u	87.9	%

The maximum voltage of an ES unit: $V_{ES\_max} = 32V$.

The voltages of an ES unit related to SoC: $V_{SoC_l} = 20V$; $V_{SoC_{nl}} = 22V$; $V_{SoC\_nu} = 28V$; $V_{SoC\_u} = 30V$.

Ideally, charge or discharge can be determined based on the direction of measured i_L or i_o compared to 0. However, the current ripples will introduce difficulty and cause oscillation. Instead, I_o* is used and compared to 0, and thus the indicator s0 is obtained, as shown in Fig 4.15. I_o* is dependent on the bus/load voltage and has much smaller ripples. Use s1 to s4 to determine the region of SoC in Fig 4.13. The formula used to calculate k_{SoC} is chosen based on these five indicators through multiplexers in (4.7).

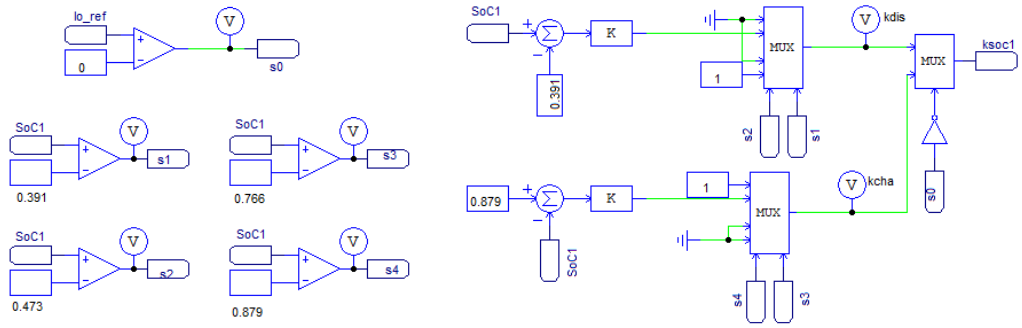

Fig 4.15 Implementation of SoC control in PSIM

Chapter 5 Performance Verification in Simulations

The designed control strategy is verified in simulations. First, analog primary control for an ES unit is validated. Then, analog primary control, SoC control, and secondary control is validated in the proposed isolated DC Nanogrid. Finally, the digital secondary control with communication delay is tested in the Nanogrid.

5.1 Primary Control with One ES Unit

Supercapacitors (SCs) are used as ES unit. The primary control includes inner current control and current-mode droop control. In droop control, the output voltage of the converter v_o is measured, and the output current reference I_{o_ref} is generated to let the ES unit supply or absorb a certain amount of power. The output current i_o is controlled indirectly by the input/inductor current i_L and a dynamic current gain k_{ioL}. i_L is controlled in the inner current loop. k_{ioL} presents the ratio between i_L and i_o to achieve accurate output power at steady state. $k_{ioL} = \frac{v_o}{v_{Es}}$, and $I_{L\_ref} = k_{ioL} I_{o\_ref}$.

The power stage and the control block are as below.

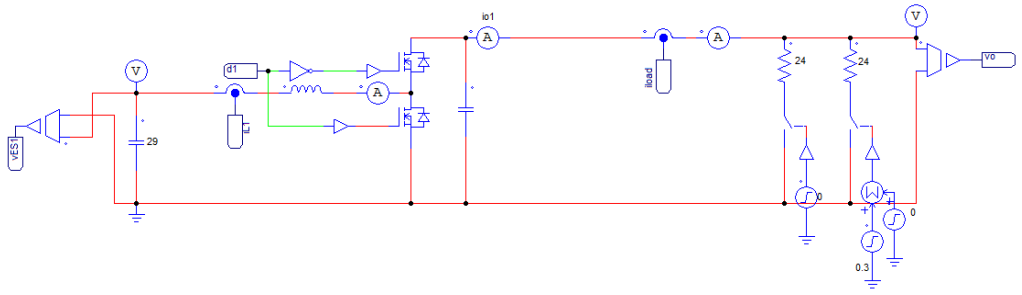

Fig 5.1 Power stage of one ES unit

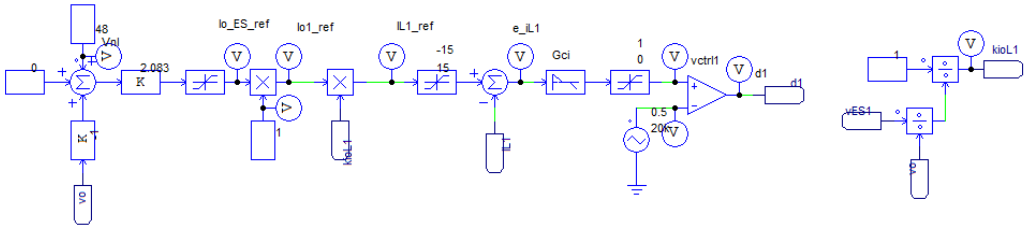

Fig 5.2 Primary control block of one ES unit

The resistive load R_o changes from 24Ω to 12Ω at time 0.3s, and the transient is shown in Fig 5.3. The output current i_o suddenly increases accordingly. Then the output voltage v_o gradually decreases. According to droop control, the reference of the output current I_{o_ref} increases with a decreasing voltage as well as the reference of the inductor current I_{L_ref} through k_{ioL}. The actual inductor current i_L follows I_{L_ref} very quickly. Considering ripples of i_L and I_{L_ref}, use their average values to calculate the transient characteristics of the inner current loop. Settling time $t_{set} = 0.552ms$ regarding a 2% difference of the steady-state value. Although I_{L_ref} keeps changing afterward, i_L is regarded at steady state. At around 20ms, v_o reaches steady state.

In droop control, if an ES unit is supplying power, the output voltage v_o is always smaller than V_{nl}. With an increase in load demand, the output power of the ES unit v_o decreases. The system is stable and can settle fast without undershoot or overshoot.

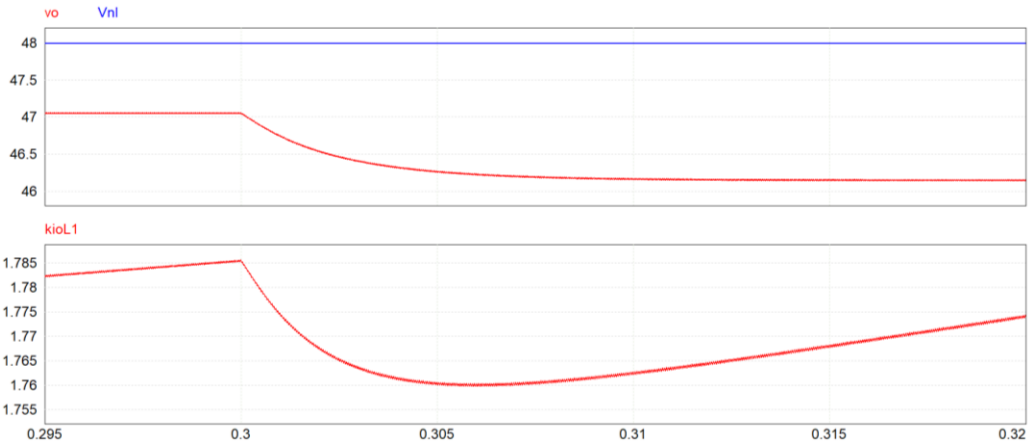

Fig 5.3.a) Simulation results in transient: v_o, V_{nl}, and k_{ioL1}

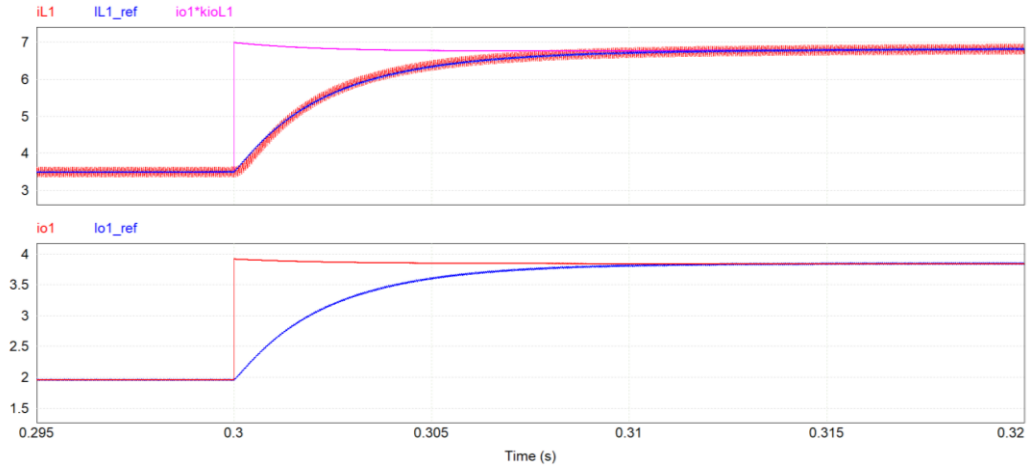

Fig 5.3.b) Simulation results in transient: i_{L1}, I_{L1_ref}, $i_{o1}k_{ioL}$, i_{o1}, and I_{o1_ref}

At steady state, because of an increasing k_{ioL} (decreasing v_{ES} due to discharge), i_L keeps increasing but v_o stays the same as well as i_o, as shown in Fig 5.4.

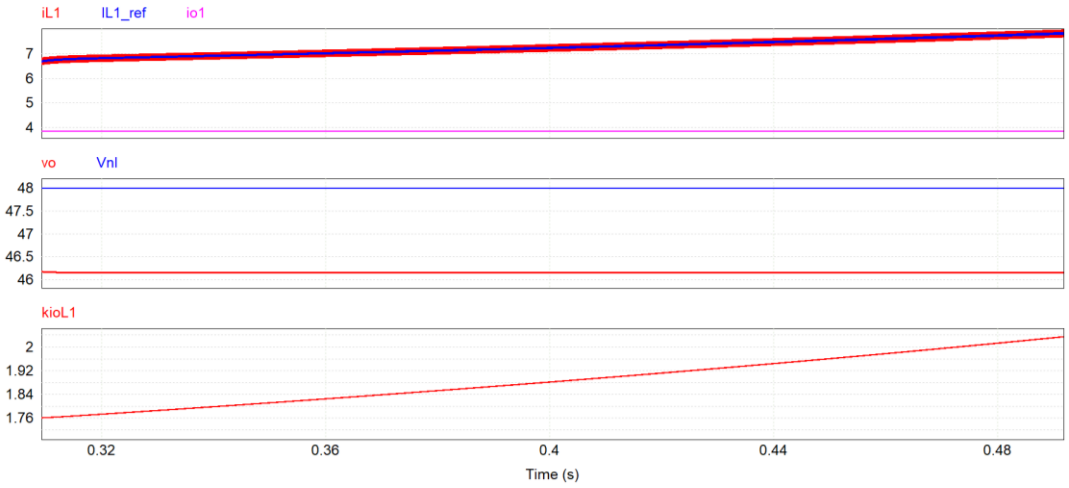

Fig 5.4 Simulation results at steady state: v_o, V_{nl}, i_{L1}, I_{L1_ref}, i_{o1}, and k_{ioL1}

At the first steady state before 0.3s, average actual values: $v_{o\_AV} = 47.058V$, and $i_{o\_AV} = 1.961A$. Since $R_o = 24\Omega$ and use the droop formula, the calculated values: $v_{o\_c} = 47.064V$, and $i_{o\_c} = 1.961A$. The power error is -0.012W. At the second steady state after 0.3s, $v_{o\_AV} = 46.152V$, and $i_{o\_AV} = 3.846A$. The calculated values: $v_{o\_c} = 46.152V$, and $i_{o\_c} = 3.846A$ with $R_o = 12\Omega$. The power error is zero.

Although an indirect current control is employed where i_o is controlled through i_L and a dynamic ratio k_{ioL}, the power error is very small at steady state and neglectable. Accurate power-sharing control is obtained.

5.2 Primary Control in Isolated DC Nanogrid

The Nanogrid includes two ES units, one PV unit, and five resistive loads. The PV unit, its converter, and controller are combined and simplified as one model discussed previously. The power stage is as below.

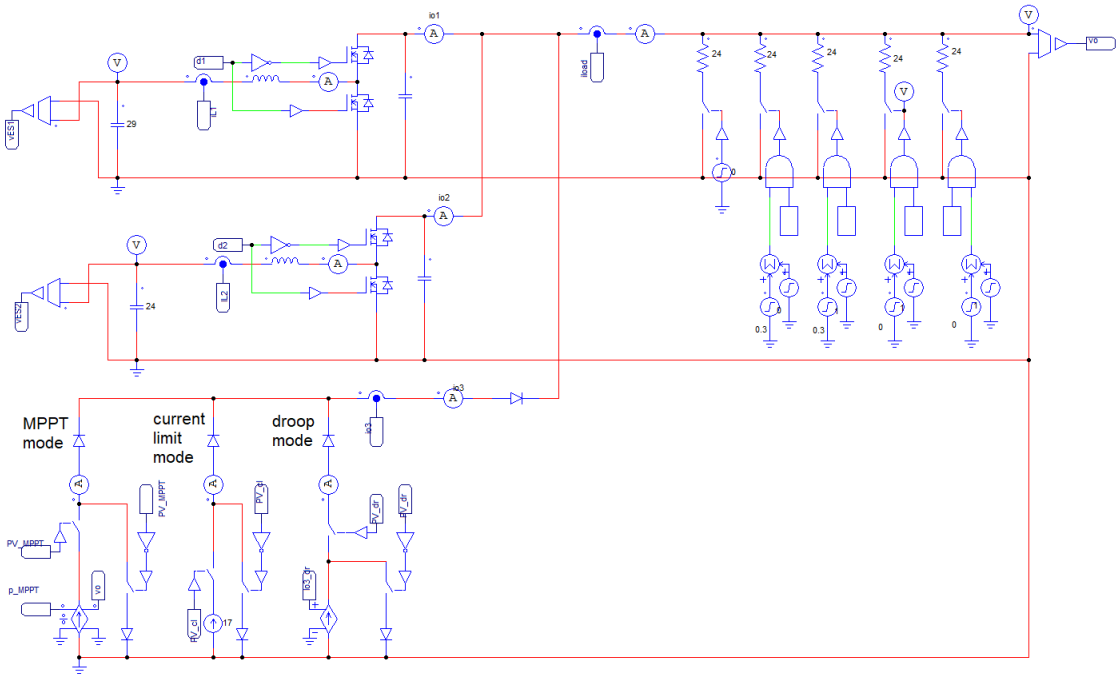

Fig 5.5 Power stage of Nanogrid

The test profile is as below. And the following test uses the same profile. The approximate load power is computed at the rated DC bus voltage. The initial SoC of the two ES units are SoC_1 = 82.1% and SoC_2 = 56.3%. Only primary control of the Nanogrid is activated. The simulation results are as below.

Table 5.1 Test profile

Segment (#)	Time (s)	# of loads	Approx. P_{load} (W)	P_{MPPT} (W)
1	0.0 – 0.1	3	288	300
2	0.1 – 0.3	3	288	150
3	0.3 – 0.6	5	480	150
4	0.6 – 1.0	5	480	500
5	1.0– 1.2	2	192	500
6	1.2 –1.6	2	192	800

At 0.1s, P_{MPPT} decreases, the output power of ES units P_{o1} and P_{o2} increase and the bus volage v_o decreases. At 0.3s, load power P_{load} increases, P_{o1} and P_{o2} increase again with a decreased v_o. If the output power or the currents of ES units increases, the voltage will decrease while discharging in droop control. If ES units are discharging, $v_o < V_{nl}$.

At 0.6s, P_{MPPT} increases and is slightly larger to P_{load}, the ES units start to charge, and v_o climbs to a little larger than V_{nl}. If ES units are charging, $v_o > V_{nl}$ in droop control. At 1s, P_{load} largely falls, thus ES units are charged with larger currents, and v_o increases. At 1.2s, P_{MPPT} increases again, P_{o1} and P_{o2} increase, causing an even larger v_o. The magnitude of the current reference for ES units $I_{o\_ES\_ref}$ increases until it reaches its limit -5A at 1.205s, and ES units enter the current limit region. At 1.209s, v_o reaches the upper voltage of the MPPT region $v_{o\_MPPT\_uv}$, and the PV unit enters the droop region ($PV_{mode} = 0$) from MPPT region ($PV_{mode} = 1$) leading to a fast falling output current of the PV unit i_{o3}. The droop region of PV makes v_o always smaller than V_{o_max} in primary control and thus provide overvoltage control. v_o varies between 46.442V to 51.161V the entire period.

The designed droop control strategy for the Nanogrid functions successfully. Energy sources can share the load demand, and the transitions of their control modes are smooth. Note that SoC of ES unit 1 is over 100% which is not allowed. And SoC should be kept within a designed range the whole time.

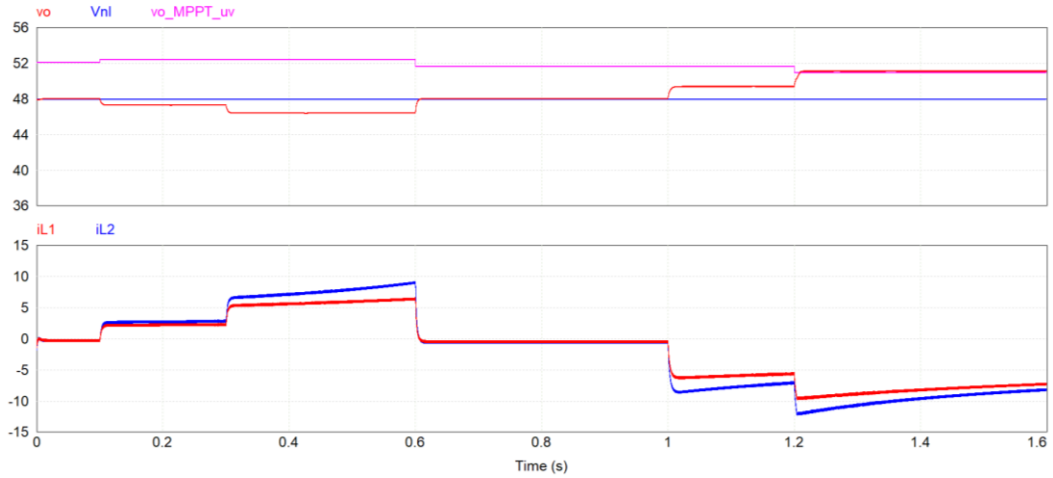

Fig 5.6.a) Simulation results of primary control in Nanogrid: v_o, V_{nl}, $v_{o\_MPPT\_uv}$, i_{L1} and i_{L2}

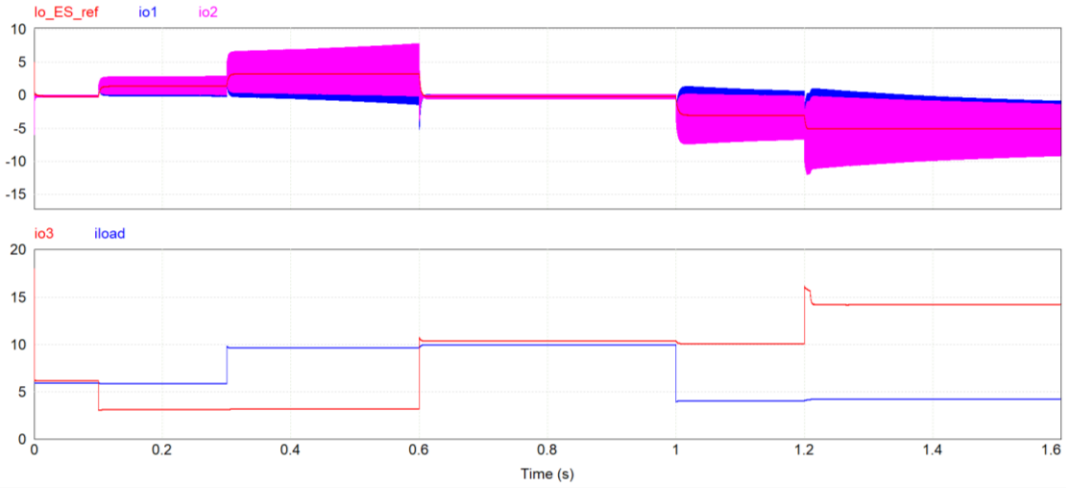

Fig 5.6.b) Simulation results of primary control in Nanogrid: $I_{o\_ES\_ref}$, i_{o1}, i_{o2}, i_{o3} and i_{load}

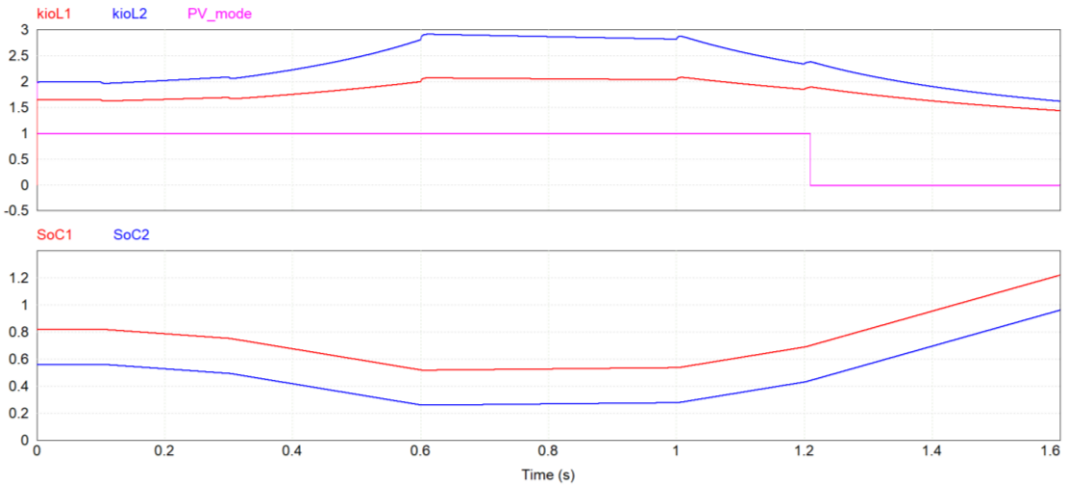

Fig 5.6.c) Simulation results of primary control in Nanogrid: k_{ioL1}, k_{ioL2}, PV_{mode}, SoC_1 and SoC_2

As desired, the output power of two ES units should be equal. The average values of currents are measured in two switching cycles to avoid the impact of change of k_{ioL}, as shown in Fig 5.7. the output currents $i_{o1_{AV}} = 3.24A$, and $i_{o2_{AV}} = 3.21A$. The inductor currents $i_{L1\_AV} = 5.93A$, and $i_{L2\_AV} = 7.82A$. Although the ES units have different initial SoC or v_{ES}, the current error between i_{o1_AV} and i_{o2_AV} is 30mA. The output power is as desired and power-sharing is accurate. Since there are multiple output capacitors, the current harmonics from ES unit 1 will go through C_{o1} and also C_{o2}, leaving harmonics in i_{o1}. However, the load current has very few harmonics. If ES units are seen as a storage bank, it has no significant ripples in its output current.

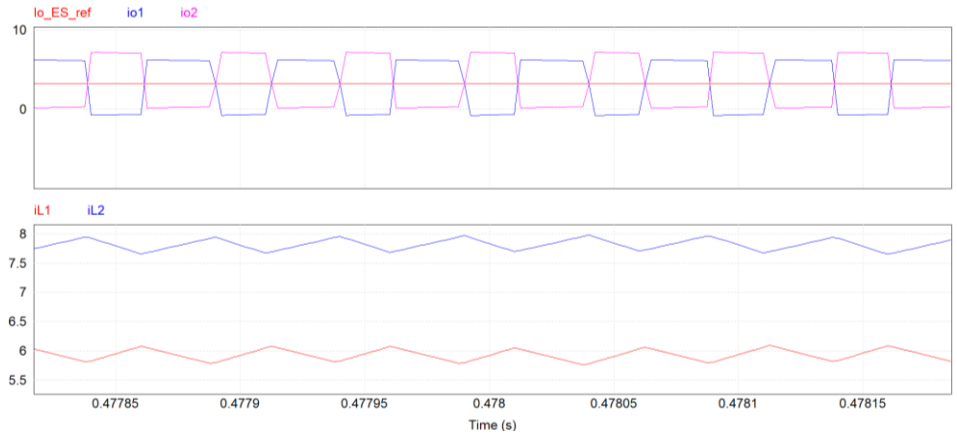

Fig 5.7 Detailed simulation results of primary control in Nanogrid: $I_{o\_ES\_ref}$, i_{o1}, i_{o2}, i_{L1} and i_{L2}

Using the same test profile and controller, the following test verifies a smaller output capacitor might destabilize the system. The only difference is that the output capacitor is 1mF, smaller than C_o but much larger than the traditionally calculated value.

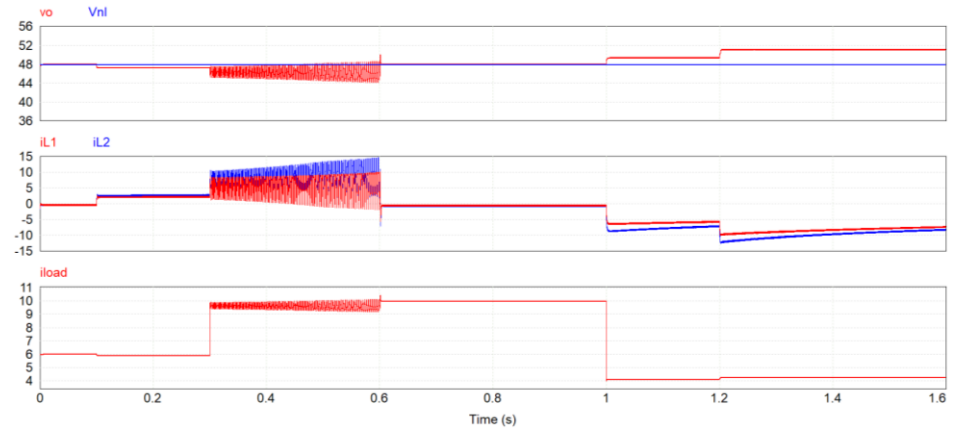

Fig 5.8 Detailed simulation results of primary control in Nanogrid with output capacitor of 1mF: v_o, V_{nl}, i_{L1}, i_{L2} and i_{load}

The power for each ES unit is approximately 165W, from 0.3s to 0.6s. Apparently, the system cannot be stable with large currents or heavy loads, where the RHP zero has a large impact. The design approach for output capacity is also validated.

5.3 Primary Control and SoC Control in Isolated DC Nanogrid

As mentioned before, if SoC reaches SoC_{nl} while discharging, an ES unit enters SoC control with a linearly decreasing output current until it reaches SoC_l where the ES unit stops discharging. if SoC reaches SoC_{nu} while charging, an ES unit enters SoC control with a linearly decreasing magnitude of output current until it reaches SoC_u, and the ES unit stops charging. The same test profile is used here. The simulation results are as below.

At 0.336s, ES unit 2 activates SoC control where $SoC_2 = SoC_{nl}$, and k_{SoC2} decreases from 1. $I_{o2\_ref} = k_{SoC2} I_{o\_ES\_ref}$. A falling I_{o2_ref} leads to a falling I_{L2_ref} and i_{L2}. v_o starts to decrease due to a decrease in the power. Due to droop control, $I_{o\_ES\_ref}$ increases as well as i_{L1} through k_{ioL1}, however it cannot make up for the loss. v_o keeps decreasing. At 0.457s, I_{o1_ref} reaches its limit 5A, and with a continuing decreasing i_{L2}, v_o drops faster. At 0.575s, ES unit 1 also enters SoC control and has a falling output current. Again, v_o drops faster. At 1.317s and 1.354s, ES units 1 and 2 enter SoC control while charging, respectively. At 1.6s, $SoC_1 = 87.5\%$, and $SoC_2 = 87.3\%$.

v_o varies from 41.423V to 52.248V. Because ES units cannot realize their full potential due to SoC control to balance the power demand of load and power supply of the PV unit, v_o has a larger variation than the previous test.

According to SoC control, the output current and the inductor current of an ES unit can be controlled by k_{SoC} to keep SoC within a designed range. In addition, the difference of SoC has been largely reduced and even neglectable at 1.6s. SoC control helps balance SoC of multiple ES units.

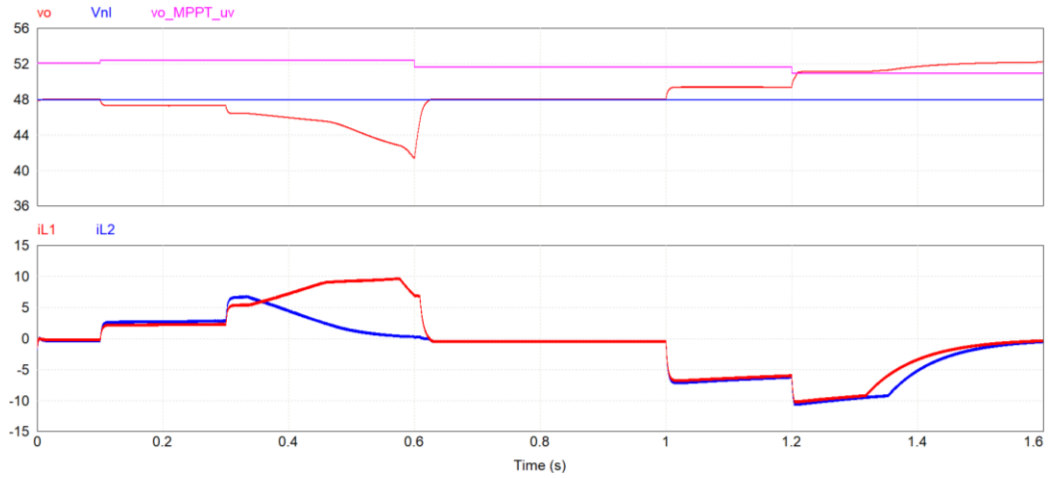

Fig 5.9.a) Simulation results of primary control and SoC control in Nanogrid: v_o, V_{nl}, $v_{o\_MPPT\_uv}$, i_{L1} and i_{L2}

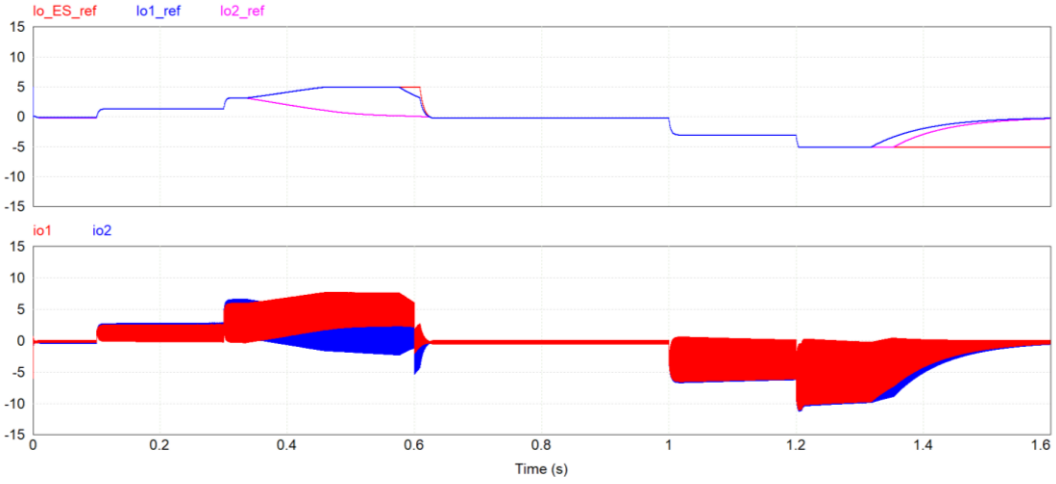

Fig 5.9.b) Simulation results of primary control and SoC control in Nanogrid: $I_{o\_ES\_ref}$, I_{o1_ref}, I_{o2_ref} , i_{o1} and i_{o2}

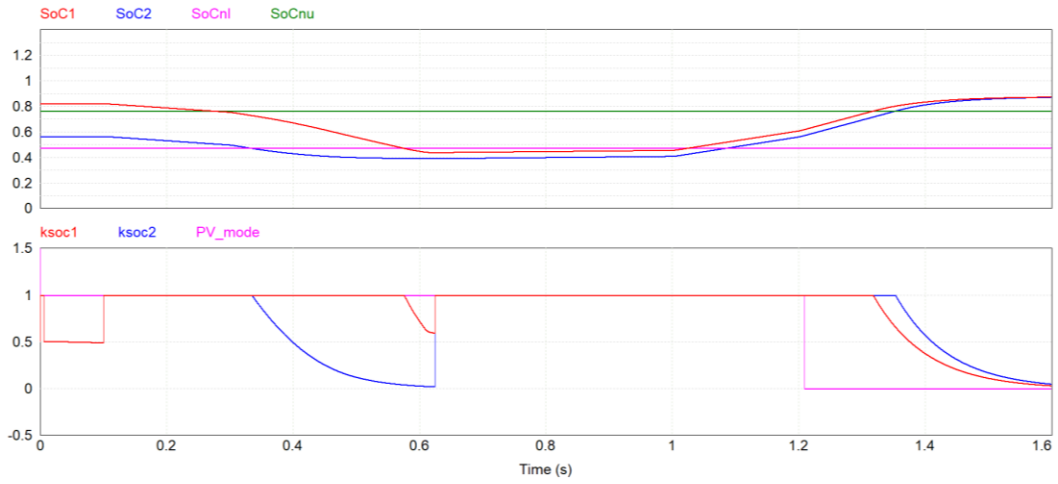

Fig 5.9.c) Simulation results of primary control and SoC control in Nanogrid: SoC_1, SoC_2, SoC_{nl}, SoC_{nu}, k_{ioL1}, k_{ioL2} and PV_{mode}

5.4 Secondary Control in Isolated DC Nanogrid

Secondary control composes SoC control of ES units and voltage regulation. The control block of voltage regulation is shown below. An anti-windup is employed to avoid building up the voltage error, especially when the voltage is away from its reference for a long time.

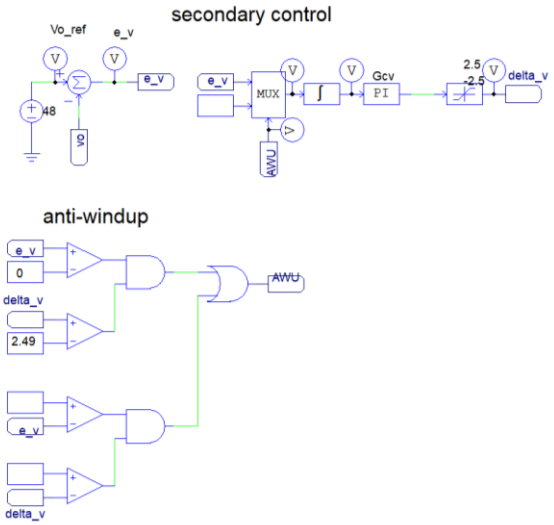

Fig 5.10 Control block of voltage regulation with anti-windup

In voltage regulation, v_o is expected to be regulated at its nominal value of 48V (V_{nl}) by a control signal δv. Most of the time, v_o should be maintained at V_{nl} at steady state. However, if δv reaches its upper or lower boundary, it is possible that $v_o \neq V_{nl}$. The simulation results are shown below.

At 0.1s, since the output power of the PV unit decreases, the Nanogrid needs power from the ES units. And in the primary droop control, if an ES unit supplies power, $v_o < V_{nl}$. The secondary control then has a positive voltage error and then generates a positive δv. It makes the ES units supply more power so that $v_o = V_{nl}$.

At 0.326s, ES unit 2 triggers SoC control. At the same time, the current from ES unit 2 keeps decreasing by k_{SoC2}. At 0.409s, although δv reaches its upper limit of 2.5V, ES unit 2 has a smaller SoC where $k_{SoC2} = 0.33$. Thus, ES units and the PV unit cannot supply enough power to maintain v_o at V_{nl}. On the other hand, since more power of ES units is consumed in voltage regulation to maintain the bus voltage, their SoC drops faster than in the previous test. And ES unit 1 enters SoC control at 0.549s (0.575s in the previous test).

At 0.6s, v_o reaches its minimum value in this test of 38.601V, smaller than that in the previous test, since more power of ES units are consumed beforehand. Note that the overshoot of v_o is observed for the first time. At 0.636s, the peak value $v_o = 49.265V$(2.64%).

Due to the surplus power, the PV unit reaches its droop region and supplies less power at 1.204s. δv reaches its lower limit of $-2.5V$ at 1.209s, and v_o settles quickly. Later, ES units activate SoC control at 1.332s and 1.353s, respectively. Since the charging power (current) is smaller, v_o starts to climb toward $V_{o_\max\ _new}$The sum of $V_{o\_\max}$ (no-load voltage of the PV unit: 52.8V) and δv. With a negative δv, the updated no-load voltage of the PV unit $V_{o\_\max\ \_new} < V_{o\_\max}$. $V_{o\_\max} + \delta v_{\min} = 50.3V$, which is the maximum value that v_o can reach theoretically with voltage regulation. At 1.6s, $v_o = 49.76V$, much smaller than the value of 52.248V in the previous test. Voltage regulation helps reduce the maximum bus voltage under light load conditions, which is still larger than V_{nl}.

In summary, voltage regulation can regulate the bus voltage at its nominal value at steady state. And it can also have a smaller maximum voltage, larger than the nominal value, with a light load due to the PV unit. However, it can consume ES units more quickly. Also, SoC control may interfere with the performance of voltage regulation.

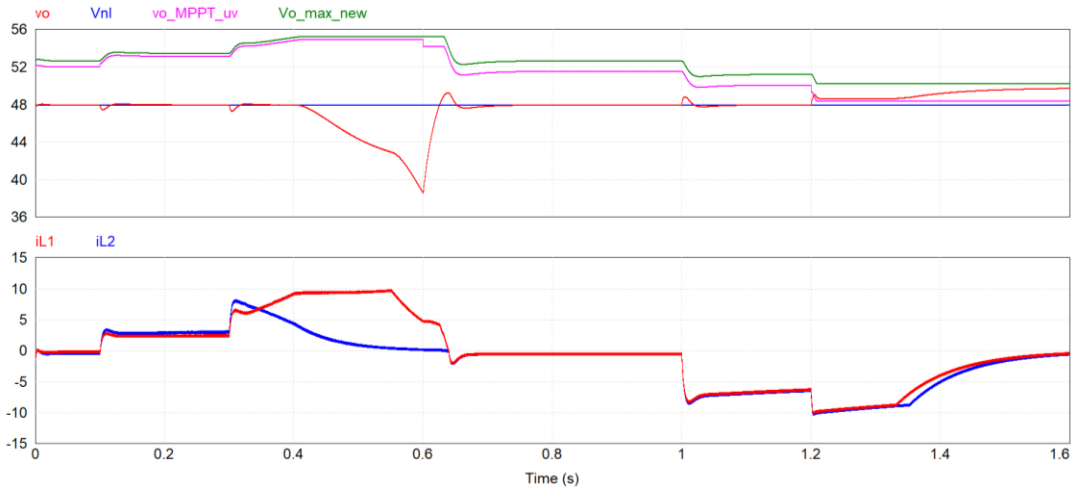

Fig 5.11.a) Simulation results of secondary control: v_o, V_{nl}, $v_{o\_MPPT\_uv}$, $V_{o\_max\_new}$, i_{L1} and i_{L2}

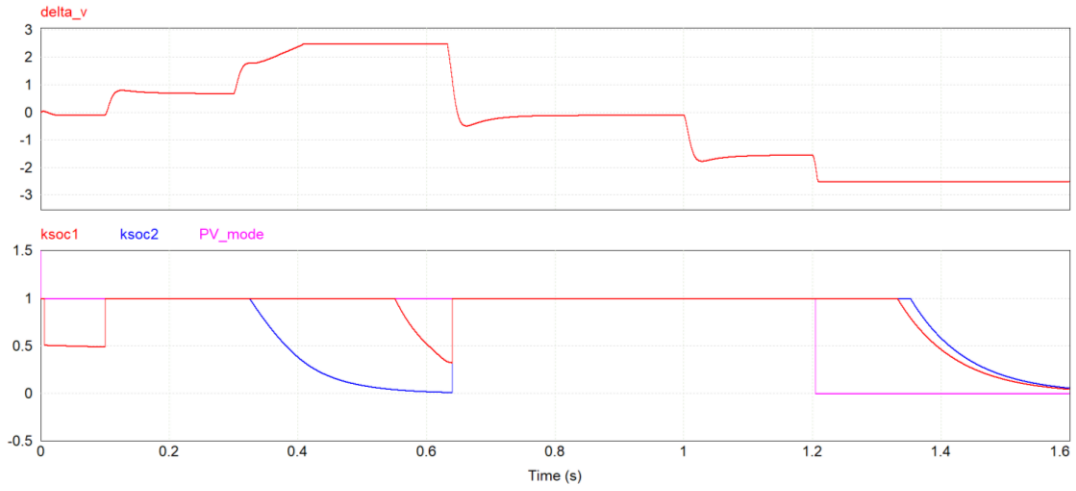

Fig 5.11.b) Simulation results of secondary control: δv, k_{SoC1}, k_{SoC2} and PV_{mode}

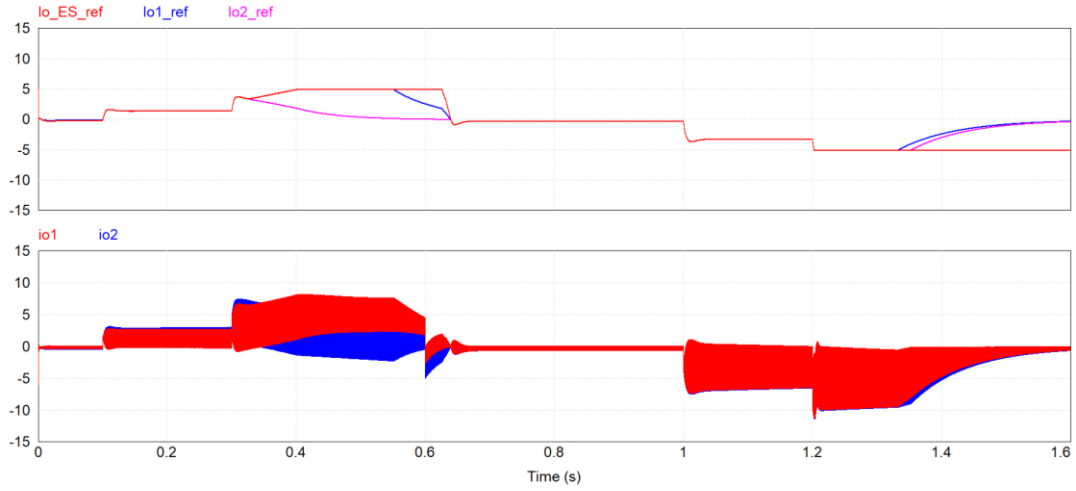

Fig 5.11.c). Simulation results of secondary control: $I_{o\_ES\_ref}$, I_{o1_ref}, I_{o2_ref}, i_{o1} and i_{o2}

5.5 Digital Secondary Control in Isolated DC Nanogrid

Digital control is implemented by digital controllers using s2z function in PSIM and Zero-Order Hold (ZOH) block for sampling. Additionally, to simulate communication, a ZOH of 500Hz and a delay of 500Hz are employed between the secondary control and primary control. It can simulate the commutation. For primary control, the sampling frequency is 20kHz same as the switching frequency. For secondary control, the sampling frequency is 500Hz.

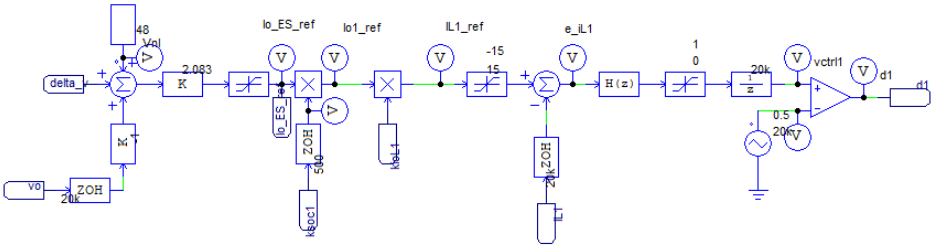

Fig 5.12.a) Modified digital primary control

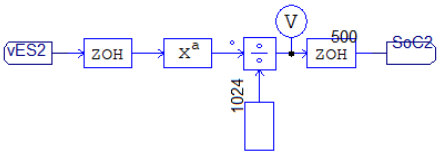

Fig 5.12.b) Modified part of digital SoC control

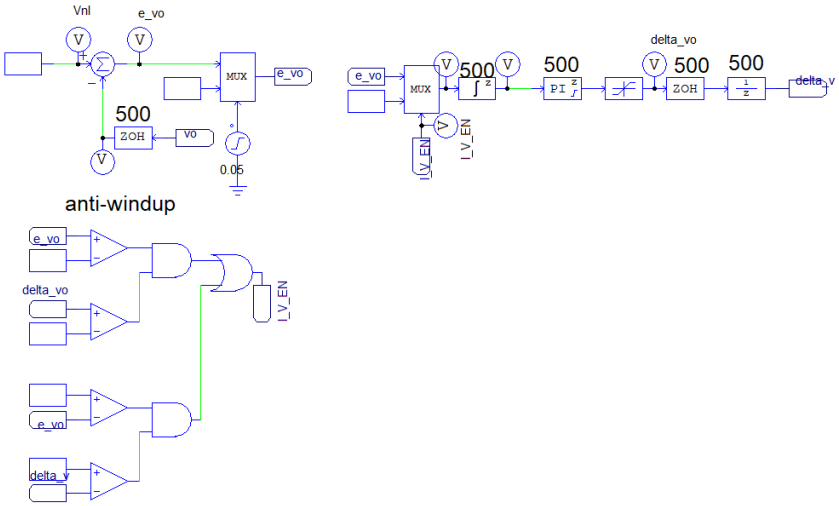

Fig 5.12.c) Modified digital voltage regulation

The simulation results are shown in Fig 5.13. The control strategy can still perform well. Note that there are some oscillations in i_L and i_{L2} during the transient due to the communication delay. If low-bandwidth communication is considered and the communication rate decreases to 100Hz [39], the simulation results are shown in Fig 5.14. The secondary controller cannot regulate the bus voltage properly.

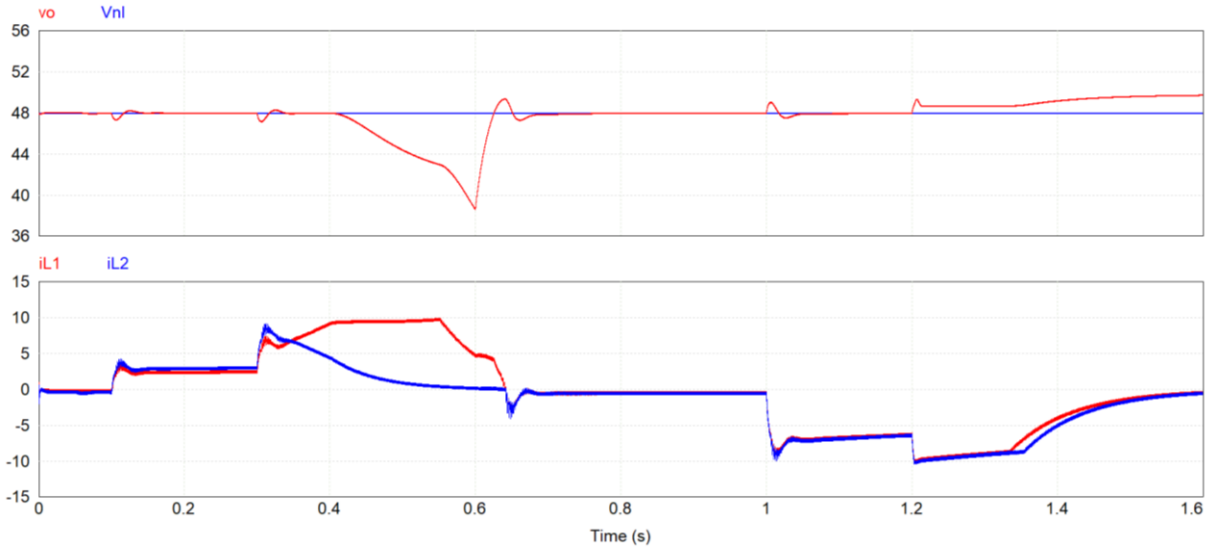

Fig 5.13 Simulation results of digital secondary control in Nanogrid with communication of 500Hz: v_o, V_{nl}, i_{L1} and i_{L2}

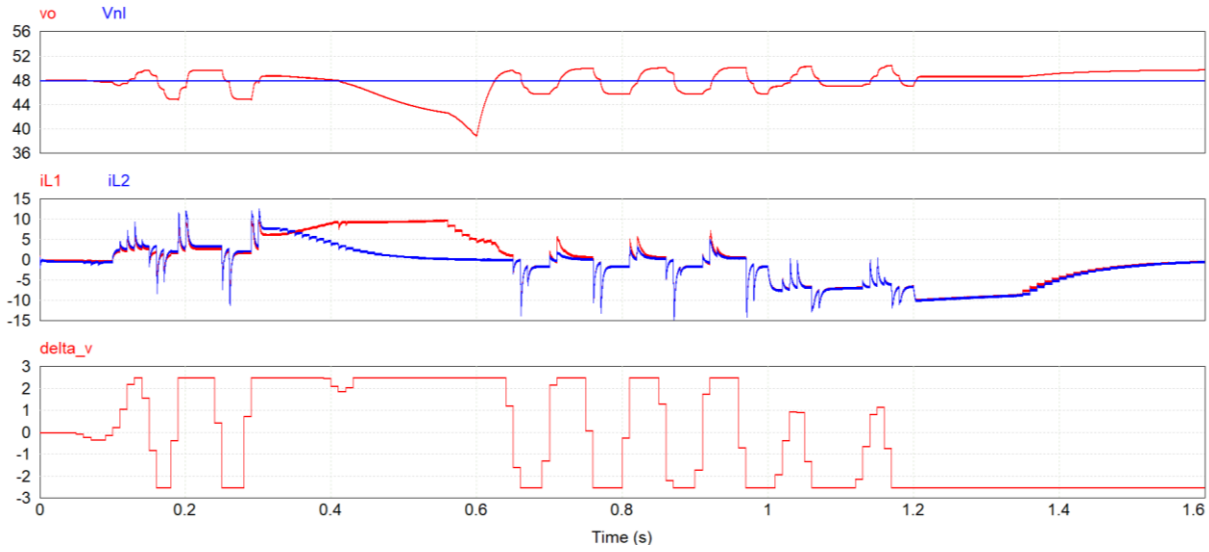

Fig 5.14 Simulation results of digital secondary control in Nanogrid with communication of 100Hz: v_o, V_{nl}, i_{L1}, i_{L2} and δv

If a delay of 100Hz is considered while the secondary controller is designed, a delay block is inserted after the controller in Fig 4.2. A new voltage controller is designed based on Bode Plots.

For smoothness in digital control, it should avoid large control steps to put significant stress on the power plant. Therefore, the sampling frequency is suggested to be 20 to 40 times of the bandwidth. The new cross-over frequency is thus set 5Hz, and the phase margin is still 60°. The secondary controller becomes an integer in series of a PI controller where $\tau_{cv} = 0.164$ and $K_{cv} = 31.623$. The simulation results are shown below.

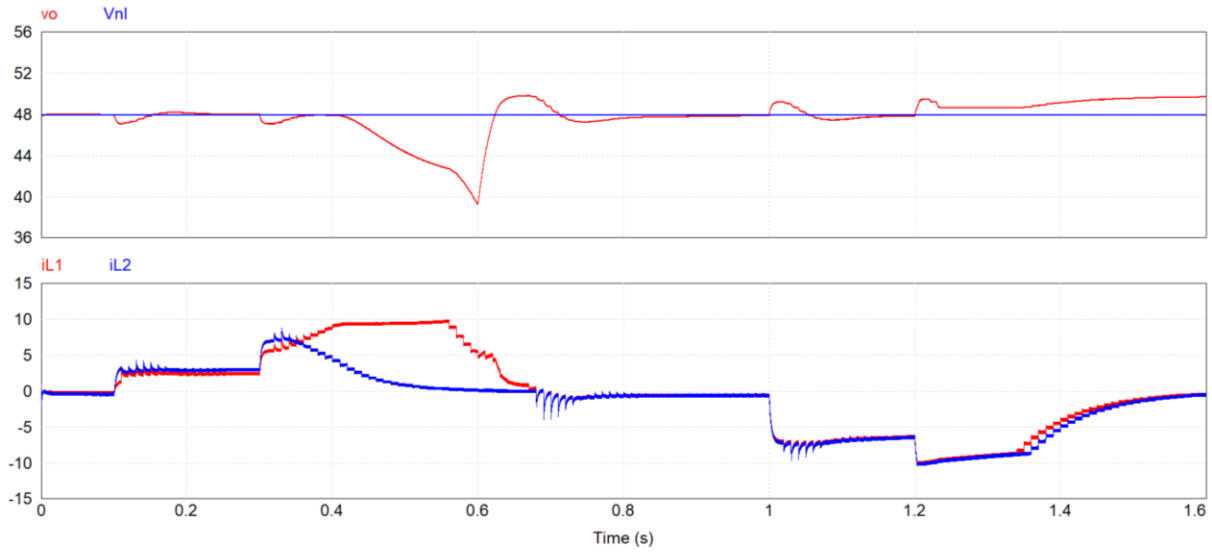

Fig 5.15.a) Simulation results of digital secondary control in Nanogrid with communication of 100Hz and a new controller: v_o, V_{nl}, i_{L1} and i_{L2}

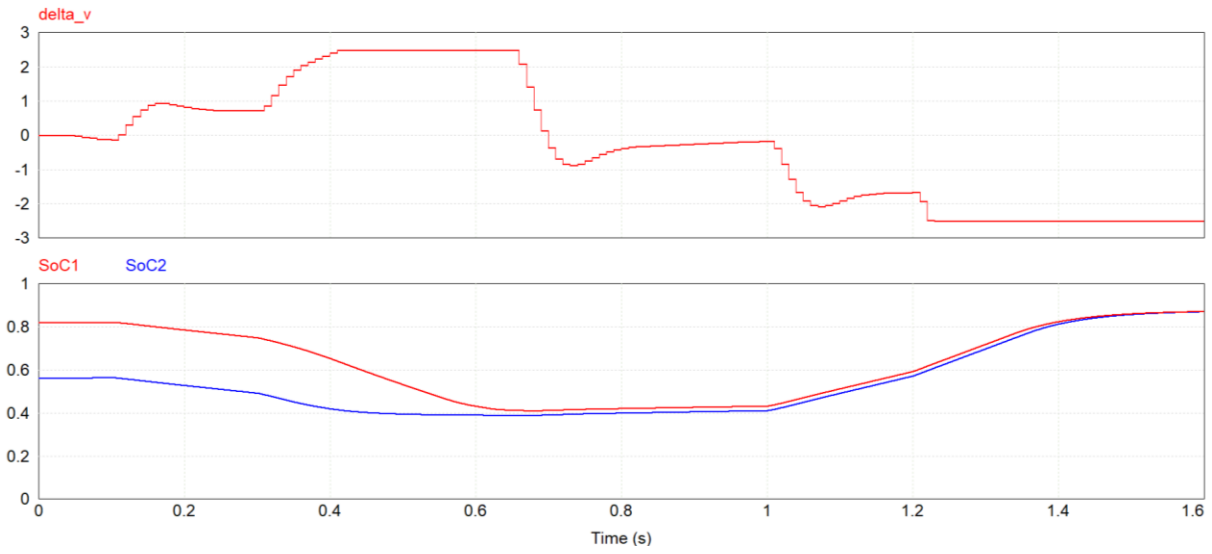

Fig 5.15.b) Simulation results of digital secondary control in Nanogrid with communication of 100Hz and a new controller: δv, SoC_1, and SoC_2

The bus voltage is well regulated, varying from 39.434V to 49.765V. SoC changes from 39.2% to 87.3% within the desired range.

The control strategy is valid in digital control.

Chapter 6 Conclusions

6.1 Summary

A hierarchical control strategy for the proposed isolated DC Nanogrid is discussed and validated in simulations of analog and digital control. Droop control is used to achieve power-sharing on the primary control level. On the secondary control level, SoC control works on the slope of the original droop control to keep SoC of ES units within a predefined range. Bus voltage regulation works on the "no-load" voltages of the PV unit and ES units in droop control to maintain the bus voltage at its nominal value at steady state. And it is also implemented on the secondary control level via communication.

Conventional Class C Boost converters are used as interfaces for ES units. Also, a traditional PI control design is employed. It is verified that these two can still work appropriately with droop control. The RHP zero due to the Class C converter is analyzed. And the caused stability issue is solved where the controllers are designed based on the worst-case scenario to ensure the stability of the Nanogrid. Moreover, a new design approach for the output capacitor of the Class C converter is introduced to deal with the unconventional loop of current-mode droop control and a random droop factor.

Chapter 2 discusses the configuration of the proposed isolated DC Nanogrid and briefly introduces the hierarchical control strategy. Droop control on the primary control level achieves power-sharing among two ES units and one PV unit, and a current ratio guarantees its accuracy at steady state. Secondary control needs communication and includes SoC control and voltage regulation. An analysis of power-sharing in droop control is given based on load variations and variations of maximum power points of the PV unit. A design approach for droop parameters is introduced, considering the acceptable range of the bus voltage and load demand. A simplified PV model combining a PV unit, its converter, and its controller for simulation is mentioned.

Chapter 3 discusses the design of primary control for ES units. Due to the RHP zero, the worst-case scenario in terms of stability happens when the load demand is heaviest, and the voltage gain of the converter is largest. The quiescent operating point is chosen to be the worst-case scenario based on which a primary PI type 2 controller is designed such that the system can stabilize under considered conditions. Also, based on the operating point, the output capacitor of the converter is

designed to stabilize primary control with a random droop factor and to yield a predefined settling time. The primary control response of an ES unit to a step input of the secondary control signal presents internal stability with the existence of secondary control (voltage regulation). Also, the primary control response to a step input of the load current shows its stability to load variations. The step responses show that the system can stabilize with the designed controller and the output capacitor.

Chapter 4 introduces voltage regulation in the Nanogrid. A voltage controller is designed. Two models of the Nanogrid are compared: original one ES-unit model and equivalent one ES-unit model. According to the simulation results, the former can represent the Nanogrid slightly better. SoC control is designed to keep SoC of ES units within a predefined range and to balance SoC of multiple ES units.

Chapter 5 presents the simulation results of analog control under different circumstances validating the designed control strategy in PSIM. It is also verified by digital control simulations considering the communication.

6.2 Future Work

Some of the suggestions for future work related to this study are as follows.

- An experiment test can be used to validate the control strategy in the isolated DC Nanogrid.
- Undervoltage Load Shedding can be designed to tackle undervoltage scenarios in the isolated Nanogrid. Or fuel cells can be used as backup storage to supply power in the long term.
- Supercapacitors are used as ES units in the thesis. Batteries have more complex characteristics and can be tested in the future.

References

[1] "Economic Benefits of Increasing Electric Grid Resilience to Weather Outages," Executive Office of the President, August 2013, https://www.energy.gov/downloads/economic-benefits-increasing-electric-grid-resilience-weather-outages.

[2] "SMART GRID: Program Overview, "Natural Resources Canada, 2020, https://www.nrcan.gc.ca/climate-change/green-infrastructure-programs/smart-grids/19793.

[3] D. Burmester, R. Rayudu, W. Seah and D. Akinyele, "A review of nanogrid topologies and technologies," *Renewable and Sustainable Energy Reviews*, vol. 67, 2017, pp. 760-775.

[4] Muyeen SM, Islam SM and Blaabjerg F, "Variability, Scalability and Stability of Microgrids," London, United Kingdom: Institution of Engineering and Technology, 2019.

[5] https://www.nrcan.gc.ca/energy-efficiency/homes/canada-greener-homes-grant/23441.

[6] "Renewables 2020-Analysis and forecast to 2025," International Energy Agency, https://www.iea.org/reports/solar-pv.

[7] D. Feldman, V. Ramasamy, R. Fu, A. Ramdas, J. Desai and R. Margolis, "U.S. Solar Photovoltaic System and Energy Storage Cost Benchmark: Q1 2020," National Renewable Energy Laboratory, https://www.nrel.gov/docs/fy21osti/77324.pdf.

[8] "Frustrated with utilities, some Californians are leaving the grid," *New York Times*, Mar. 13, 2022.

[9] M. C. di Piazza, M. Luna, M. Pucci, G. L. Tona and A. Accetta, "Electrical Storage Integration into a DC Nanogrid Testbed for Smart Home Applications," *2018 IEEE International Conference on Environment and Electrical Engineering and 2018 IEEE Industrial and Commercial Power Systems Europe (EEEIC / I&CPS Europe)*, 2018, pp. 1-5.

[10] S. K. Kollimalla, M. K. Mishra, A. Ukil and G. H. Beng, "DC grid voltage regulation using new HESS control strategy," *2017 IEEE Power & Energy Society General Meeting*, 2017, pp. 1-1.

[11] S. K. Sahoo, A. K. Sinha and N. K. Kishore, "Control Techniques in AC, DC, and Hybrid AC–DC Microgrid: A Review," in *IEEE Journal of Emerging and Selected Topics in Power Electronics*, vol. 6, no. 2, pp. 738-759, June 2018.

[12] J. A. Qureshi, T. T. Lie, K. Gunawardane and N. Kularatna, "AC and DC House Wiring Efficiency Estimations using Mathematical Modelling Approach," *2021 31st Australasian Universities Power Engineering Conference (AUPEC)*, 2021, pp. 1-6.

[13] A. Gupta, S. Doolla and K. Chatterjee, "Hybrid AC–DC Microgrid: Systematic Evaluation of Control Strategies," in *IEEE Transactions on Smart Grid*, vol. 9, no. 4, pp. 3830-3843, July 2018.

[14] T. Morstyn, B. Hredzak and V. G. Agelidis, "Control Strategies for Microgrids with Distributed Energy Storage Systems: An Overview," in *IEEE Transactions on Smart Grid*, vol. 9, no. 4, pp. 3652-3666, July 2018.

[15] Z. Shuai, J. Fang, F. Ning and Z. J. Shen, "Hierarchical structure and bus voltage control of DC microgrid, Renewable and Sustainable Energy Reviews, " vol. 82, no. 3, 2018, pp: 3670-3682.

[16] R. Aryan, R. Ranjan and A. Kumar, "Primary Control Strategies for Power Sharing and Voltage Regulation in DC Microgrid: A Review," *2020 3rd International Conference on Energy, Power and Environment: Towards Clean Energy Technologies*, 2021, pp. 1-6.

[17] P. Odo, "A Comparative Study of Single-phase Non-isolated Bidirectional dc-dc Converters Suitability for Energy Storage Application in a dc Microgrid," *2020 IEEE 11th International Symposium on Power Electronics for Distributed Generation Systems (PEDG)*, 2020, pp. 391-396.

[18] T. L. Nguyen, J. M. Guerrero and G. Griepentrog, "A Self-Sustained and Flexible Control Strategy for Islanded DC Nanogrids Without Communication Links," *IEEE*

Journal of Emerging and Selected Topics in Power Electronics, vol. 8, no. 1, pp. 877-892, March 2020.

[19] B. Otomega, M. Glavic and T. Van Cutsem, "Distributed Undervoltage Load Shedding," *IEEE Transactions on Power Systems*, vol. 22, no. 4, pp. 2283-2284, Nov. 2007.

[20] R. Saxena, M. Thalari, V. Sonti and P. Chaturvedi, "Design and Power Management of Low Voltage DC Nanogrid for Solar PV/Fuel Cell fed Residential Complexes," *2021 IEEE 2nd International Conference on Smart Technologies for Power, Energy and Control (STPEC)*, 2021, pp. 1-6.

[21] B. Xu, A. Oudalov, A. Ulbig, G. Andersson and D. Kirschen, "Modeling of lithium-ion battery degradation for cell life assessment," *2017 IEEE Power & Energy Society General Meeting*, 2017, pp. 1-1.

[22] K. Bellache, M. B. Camara and B. Dakyo, "Supercapacitor Characterization Using Fluctuating DC Current - Impacts of State of Charge, Number of Cycle and Frequency on Cell Resistance and Capacitance," *2016 IEEE Vehicle Power and Propulsion Conference (VPPC)*, 2016, pp. 1-5.

[23] X. Lu, K. Sun, J. M. Guerrero, J. C. Vasquez, L. Huang and R. Teodorescu, "SoC-based droop method for distributed energy storage in DC microgrid applications," *2012 IEEE International Symposium on Industrial Electronics*, 2012, pp. 1640-1645.

[24] H. Li, L. Fu, Y. Zhang, X. Gao and Y. Lin, "SOC-based Hybrid Energy Storage System Dynamical and Coordinated Control for Vessel DC Microgrid," *2019 IEEE Innovative Smart Grid Technologies - Asia (ISGT Asia)*, 2019, pp. 1381-1386.

[25] C. Jamroen, S. Sirisukprasert and N. Hatti, "A Study on SoC Management of Energy Storage System for Voltage Regulation Application in Distribution Network," *2020 11th International Renewable Energy Congress (IREC)*, 2020, pp. 1-6.

[26] "IEEE Standard for the Testing of Microgrid Controllers," in *IEEE Std 2030.8-2018*, pp.1-42, Aug. 2018.

[27] H. Sabry, A. H. Shallal, H. S. Hameed and P. J. Ker, "Compatibility of household appliances with DC microgrid for PV systems," *Heliyon*, vol. 6, no. 12, 2020.

[28] V. Vossos, S. Pantano, R. Heard and R. E. Brown, "DC Appliances and DC Power Distribution: A Bridge to the Future Net Zero Energy Homes," Lawrence Berkeley National Laboratory, 2017.

[29] K. Garbesi, V. Vossos and H. Shen, "Catalog of DC Appliances and Power Systems," Lawrence Berkeley National Laboratory, 2011.

[30] S. Moussa, M. J. -B. Ghorbal and I. Slama-Belkhodja, "DC voltage level choice in residential remote area," *2018 9th International Renewable Energy Congress (IREC)*, 2018, pp. 1-6.

[31] M. Kamran, M. Bilal and M. Mudassar, "DC Home Appliances for DC Distribution System," *Mehran University Research Journal of Engineering and Technology*, Mehran University of Engineering and Technology, Jamshoro, Pakistan, 2017, 36 (4), pp.881-890.

[32] K. M. Bhargavi, N. S. Jayalakshmi, D. N. Gaonkar, A. Shrivastava and V. K. Jadoun, "A Comprehensive Review on Control Techniques for Power Management of Isolated DC Microgrid System Operation," in *IEEE Access*, vol. 9, 2021, pp. 32196-32228.

[33] Sankar U., S. S. Nag and S. K. Mishra, "A Multi-Input Single-Control (MISC) battery charger for DC nanogrids," *2013 IEEE ECCE Asia Downunder*, 2013, pp. 304-310.

[34] M. Forouzesh, Y. P. Siwakoti, S. A. Gorji, F. Blaabjerg and B. Lehman, "Step-Up DC–DC Converters: A Comprehensive Review of Voltage-Boosting Techniques, Topologies, and Applications," *IEEE Transactions on Power Electronics*, vol. 32, no. 12, pp. 9143-9178, Dec. 2017.

[35] M. -A. Dobrea, N. Arghira, M. Vasluianu, G. Neculoiu and A. -M. C. Moldoveanu, "MPPT techniques application and comparison for photovoltaic panels," *2021 23rd International Conference on Control Systems and Computer Science (CSCS)*, 2021, pp. 386-392.

[36] C. Zhang, J. Zhang, X. Ma, and Q. Feng. 2021. "Semiconductor Photovoltaic Cells (First edition 2021), " *Springer*, pp. 12-19.

[37] M. A. Akbar, 2019, "Shunt Connected Power Conditioner with Energy Storage for a Hydrogen Fuel Cell System Supplying a DC Nanogrid", Degree of Masters, Concordia University, Montreal.

[38] M. Ceraolo, G. Lutzemberger and D. Poli, "State-Of-Charge Evaluation of Supercapacitors", *Journal of Energy Storage*, vol. 11, 2017, pp. 211-218.

[39] A. B. Shyam, S. R. Sahoo, S. Anand and J. M. Guerrero, "Comparative Study of Various Communication Technologies for Secondary Controllers in DC Microgrid," *2021 9th IEEE International Conference on Power Systems (ICPS)*, 2021, pp. 1-6.